



Surface wrinkling of a film coated to a graded substrate

Rui-Cheng Liu^a, Yang Liu^{a,b,c,*}, Alain Goriely^{c,**}

^a Department of Mechanics, School of Mechanical Engineering, Tianjin University, Tianjin 300354, China

^b Tianjin Key Laboratory of Modern Engineering Mechanics, Tianjin 300354, China

^c Mathematical Institute, University of Oxford, Oxford, OX2 6GG, UK

ARTICLE INFO

Keywords:

Surface wrinkling
Graded materials
Film/substrate structures
Nonlinear elasticity
WKB method
Asymptotic analysis
Stroh formulation

ABSTRACT

We study the surface wrinkling of a stiff thin elastic film bonded to a compliant graded elastic substrate subject to compressive stress generated either by compression or growth of the bilayer. Our aim is to clarify the influence of the modulus gradient on the onset and surface pattern in this bilayer. Within the framework of finite elasticity, an exact bifurcation condition is obtained using the Stroh formulation and the surface impedance matrix method. Further analytical progress is made by focusing on the case of short wavelength limit for which the Wentzel–Kramers–Brillouin method can be used to resolve the eigenvalue problem of ordinary differential equations with variable coefficients. An explicit bifurcation condition is obtained from which the critical buckling load and the critical wavelength are derived asymptotically. In particular, we consider two distinct situations depending on the ratio β of the shear modulus at the substrate surface to that at infinity. If β is of $\mathcal{O}(1)$ or small, the parameters related to modulus gradient all appear in the higher-order terms and play an insignificant role in the bifurcation. In that case, it is the modulus ratio between the film and substrate surface that governs the onset of surface wrinkling. If, however, $\beta \gg 1$, the modulus gradient affects the critical condition through leading-order terms. Through our analysis we unravel the influence of different material and geometric parameters, including the modulus gradient, on the bifurcation threshold and the associated wavelength which can be of importance in many biological and technological settings.

1. Introduction

The wrinkling of thin layers on substrates is a universal morphological phenomenon of great importance in engineering materials and biological tissues (Li et al., 2012; Goriely, 2017). A typical set-up to study wrinkling is to consider a thin hard film coated to a soft substrate. If the film shrinks, grows, is prestrained, or the entire system is loaded, the film may develop wrinkles (Alawiye et al., 2019). This type of wrinkling morphologies appears in biological systems and is known to establish some of their physiological functions such as folds in human brain (Budday et al., 2014; Holland et al., 2018; Balbi et al., 2020) or in gastrointestinal tracts and airway walls (Balbi et al., 2015; Eskandari et al., 2013, 2016). From the viewpoint of mechanics, wrinkled or buckled shapes in skins, fruits or vegetables can be viewed as a result of a bifurcation process related to growth or aging (Kücken and Newell, 2004; Yin et al., 2010; Dai and Liu, 2014). In engineering, wrinkling in film/substrate bilayers can be used to design specific patterns that can be used to alter the optical property (van den Ende et al., 2013; Li et al., 2017; Lee et al., 2010), to regulate surface adhesion or tension (Chan et al., 2008; Yang et al., 2010; Lee et al., 2021), to optimize the wetting characteristic (Zhang et al.,

* Corresponding author at: Mathematical Institute, University of Oxford, Oxford, OX2 6GG, UK.

** Corresponding author.

E-mail addresses: tracy_liu@tju.edu.cn, liuy3@maths.ox.ac.uk (Y. Liu), goriely@maths.ox.ac.uk (A. Goriely).

2012; Sabbah et al., 2016), to assist in measuring the material properties of soft polymer networks (Stafford et al., 2004; Wilder et al., 2006; Cao et al., 2009; Chan et al., 2009), or to help design novel flexible sensors (Zhao et al., 2020; Wang et al., 2021; Lee et al., 2022). Moreover, certain surface morphologies brought by structure buckling are expected to occur and will play a positive role in some special cases, such as the creation of gecko's palm surfaces with adhesive force (Autumn et al., 2002). Therefore, it is of great significance to explore the buckling and post-buckling of film/substrate bilayers to understand and further to control multiple pattern formations.

The fundamental importance and potential applications of film/substrate bilayers have led to a flourish of work related to instability problem when, typically, both film and substrate are homogeneous materials. Early works were dedicated to determining the onset of surface instabilities induced by axial compression (Dorris and Nemat-Nasser, 1980; Shield et al., 1994; Ogden and Sotiropoulos, 1996; Bigoni et al., 1997; Steigmann and Ogden, 1997; Cai and Fu, 2000). Within the framework of nonlinear elasticity, Cai and Fu (1999) conducted both the linear and weakly non-linear analyses for a compressed neo-Hookean bilayer. The main finding is that there exists a critical value of the modulus ratio between two layers, across which a transition between supercritical and subcritical bifurcations occurs. Later, the influence of compressibility (Liu and Dai, 2014; Cai and Fu, 2019), curvature (Jia et al., 2018), pre-stretch (Song et al., 2008; Hutchinson, 2013), growth (Li et al., 2011a,b; Budday et al., 2015; Moulton and Goriely, 2011), multi-layering (Cheng et al., 2014; Wang et al., 2020; Zhou et al., 2022), viscosity (Huang and Suo, 2002; Huang, 2005), fibers (Stewart et al., 2016), and anisotropy (Im and Huang, 2008; Nguyen et al., 2020) were addressed theoretically, numerically and experimentally. In particular, Fu and Ciarletta (2015) studied the buckling and post-buckling of a film-substrate bilayer when they have similar material properties, and Hutchinson (2013) extended the analysis in Cai and Fu (1999) by considering the pre-stretch effect. Recently, Alawiye et al. (2019, 2020) revisited this classical problem as well and further explored the growth induced surface instability for which higher-order asymptotic solutions for the critical buckling loads and the amplitude equation were obtained.

In many systems, such as human airway wall (Eskandari et al., 2016; Liu et al., 2020) and hydrogels with graded cross-linking density and surface modified polydimethylsiloxane (PDMS) (Qi et al., 2018; Khare et al., 2009; Wang et al., 2016), the elastic modulus or Poisson's ratio of the substrate may be position dependent due to the spatial variation in the microstructure, leading to a graded substrate. Previous studies have looked at the initiation of surface buckling for an elastic graded half-space or block (Lee et al., 2008; Wu et al., 2013, 2014; Yang and Chen, 2017; Diab and Kim, 2014; Chen et al., 2018). In particular, Yang and Chen (2017) adopted an exponential modulus distribution and obtained an explicit bifurcation condition for a compressed block. Yet such choice for modulus functions leads to zero modulus at infinity in a half-space. For film/substrate bilayers, Cao et al. (2012) investigated surface instability of a stiff film on an elastic graded half-space. They derived an analytical solution of the critical compressive strain and the critical wavelength for power-law grading modulus and exponential grading modulus, respectively, and the post-buckling solution was studied numerically. Jia et al. (2014) established a semi-analytical finite element model to obtain the bifurcation threshold for an elastic graded cylinder covered by a stiff film under axial compression. Chen et al. (2017) further developed an analytical model for the buckling of a stiff film on a graded half-space and performed a finite element analysis to validate the analytical model as well as to investigate the post-buckling behavior.

When the material has a graded structure, the governing equations include space-dependent variable coefficients which are particularly difficult to study analytically. For this reason, most studies have resorted to numerical methods to solve the bifurcation problem. The present work is interested in analytical methods for the wrinkling problem in graded material in order to obtain a comprehensive picture on the role of geometrical and material parameters. Here, we use the fact that for thin stiff film resting on a soft graded substrate, the critical wavelength is small compared to the length of the film, indicating a large critical wavenumber (Cao et al., 2012; Chen et al., 2017). Hence, we can use the WKB Method (WKB stands for Wentzel–Kramers–Brillouin) to constructing asymptotic solutions for ordinary differential equations with small parameters (Hinch, 1991). It has been used by Fu (1998) and Ben Amar and Goriely (2005) to derive asymptotic results of buckling of spherical shells of arbitrary thickness. After that this asymptotic method was successfully applied to deal with the bifurcation analysis arising from the problems of cylindrical tubes (Sanjarani Pour and Fu, 2002; Sanjarani Pour, 2010; Liu, 2018; Jin et al., 2018), spherical shells (Houghton and Chen, 2003; Jia et al., 2018; De Pascalis et al., 2023), and bending of blocks (Coman and Destrade, 2008; Sanjarani Pour et al., 2013).

In this paper, we work within the framework of finite elasticity and study how the modulus gradient affects the critical buckling condition of a bilayer system with a graded substrate. We obtain explicit form for the critical buckling load and the corresponding critical wavenumber for the case of a compressed block and the case of a growing bilayer as shown in Fig. 1. In Section 2, we characterize the primary deformation prior to surface instability and present the incremental theory under in-plane compression and restricted growth. A linear bifurcation analysis is carried out using the Stroh formulation and the surface impedance matrix method in Section 3. We use WKB method to obtain an explicit bifurcation condition in Section 4. The asymptotic solutions are established in Section 5 for β small or of $\mathcal{O}(1)$ where β is the ratio of the shear modulus of the surface of the substrate to that at infinity. The reverse case where β is large is explored in Section 6.

2. Theoretical model

We consider a film/substrate bilayer composed of incompressible hyperelastic materials under compression or growth. The shear modulus of the substrate is assumed to decrease or increase uniformly in the thickness direction (away from the film). We assume that the bilayer is in a state of plane-strain deformation and therefore restrict our attention to the planar problem as shown in Fig. 1. The origin O is located at the left end of the film surface, and the X_1 - and X_2 -axes correspond to the length and depth directions, respectively. We denote the initial length of the bilayer by L and the initial thickness of the film by h_0 . The substrate is assumed to

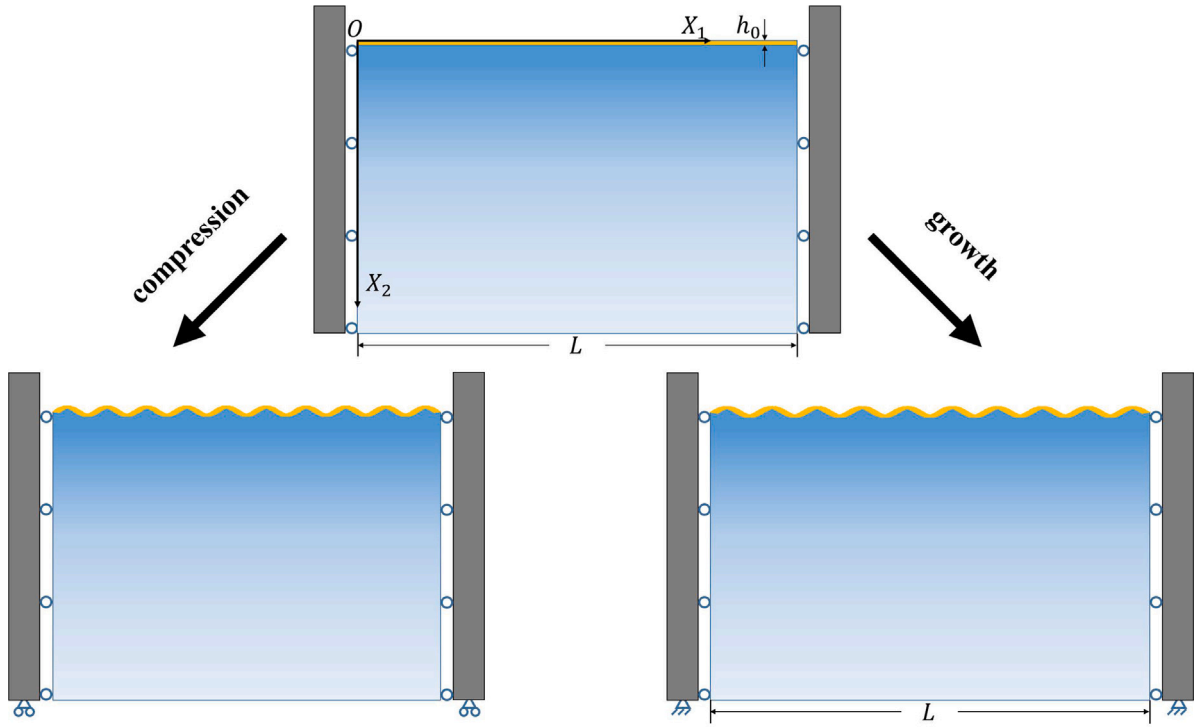


Fig. 1. Schematic illustration of a film coated to a graded half-space under uniaxial compression or growth. The initial length of the bilayer is L and the thickness of the film is h_0 . In both loading cases, the sliding end conditions are used such that there is no shear stress components in the two ends. In addition, the length L is fixed in the growth scenario so the stress is induced by restricted growth.

be a half-space. Therefore, in the reference configuration the body B_0 occupies a region $[0, L] \times ([0, h_0] \cup [h_0, \infty))$, and any material point can be represented in the orthonormal basis $\{\mathbf{e}_1, \mathbf{e}_2\}$ by its initial position $\mathbf{X} = X_1 \mathbf{e}_1 + X_2 \mathbf{e}_2$.

We assume that the film surface ($X_2 = 0$) is traction-free and that there is no displacement as $X_2 \rightarrow \infty$. On the vertical sides, the bilayer is allowed to slide along but not penetrate the sides at $X_1 = 0$ and L . We assume perfect bonding of the interface ($X_2 = h_0$) so that both traction and displacement are continuous across this interface.

When loads are applied through either uniaxial compression or growth, the bilayer undergoes a finite deformation and the resulting configuration, denoted by B_r , occupies the region $[0, l] \times ([0, h] \cup [h, \infty))$ for the compression case or within the region $[0, L] \times ([0, h] \cup [h, \infty))$ for the growth case. The position of a point originally at \mathbf{X} is now $\mathbf{x}(\mathbf{X}) = x_1 \mathbf{e}_1 + x_2 \mathbf{e}_2$. The deformation gradient associated with the deformation $B_0 \rightarrow B_r$ is given by

$$\mathbf{F} = \frac{\partial \mathbf{x}}{\partial \mathbf{X}}. \quad (2.1)$$

As the applied external load reaches a critical value, surface wrinkling may emerge as a bifurcation and this state is referred to as B_t . Since there are two layers in the model, we use an upper hat for any quantity belonging to the film and no hat otherwise. For example, \hat{W} represents the strain-energy function for the film while the strain-energy function for substrate is written as W . Since the derivations of the governing equations are similar for both layers, we only show explicitly the computation for the substrate. The equations for film are obtained by changing variables.

We consider two loading scenarios, namely, uniaxial compression and restricted growth. In both cases, we will first characterize analytically the base state B_r and then derive the linearized incremental governing equations from $B_r \rightarrow B_t$.

2.1. Uniaxial compression

In the compression case, the deformation gradient (2.1) for the base state B_r reduces to

$$\mathbf{F} = \lambda_1 \mathbf{e}_1 \otimes \mathbf{e}_1 + \lambda_2 \mathbf{e}_2 \otimes \mathbf{e}_2, \quad (2.2)$$

where λ_1 and λ_2 are the principal stretches. The incompressibility condition $\det \mathbf{F} = 1$ implies $\lambda \equiv \lambda_1 = \lambda_2^{-1}$ and the length and height of this deformed body are:

$$l = \lambda L, \quad h = h_0 / \lambda. \quad (2.3)$$

Denoting the strain–energy function of the substrate by $W = W(\mathbf{F})$ or, with a slight abuse of notation, in terms of the principal stretches by $W(\lambda_1, \lambda_2)$, the Cauchy stress tensor σ in B_r is given by

$$\sigma = \mathbf{F} \frac{\partial W}{\partial \mathbf{F}} - p\mathbf{I}, \quad (2.4)$$

where p is the Lagrange multiplier enforcing the incompressibility condition and \mathbf{I} is the second-order identity tensor. Neglecting body forces, the equilibrium equation for a static problem is:

$$\text{div } \sigma = \mathbf{0}, \quad (2.5)$$

where ‘div’ is the divergence operator in the current configuration. From the traction-free boundary condition on $x_2 = 0$ and the continuity condition on the interface $x_2 = h$, we obtain

$$\hat{p} = \lambda^{-1} \hat{W}_2, \quad p = \lambda^{-1} W_2, \quad (2.6)$$

where $W_2 = \partial W / \partial \lambda_2$.

2.2. Restricted growth

In this scenario, the length between the two rigid plates in Fig. 1 is fixed to be L and the deformation is induced by growth. We refer to the theory of volumetric growth (Goriely, 2017) that uses a multiplicative decomposition of (2.1):

$$\mathbf{F} = \mathbf{A}\mathbf{G}, \quad (2.7)$$

where \mathbf{A} is an elastic deformation tensor and \mathbf{G} is the growth tensor. We assume that both \mathbf{A} and \mathbf{G} are diagonal tensors such that

$$\mathbf{A} = \alpha_1 \mathbf{e}_1 \otimes \mathbf{e}_1 + \alpha_2 \mathbf{e}_2 \otimes \mathbf{e}_2, \quad \mathbf{G} = g_1 \mathbf{e}_1 \otimes \mathbf{e}_1 + g_2 \mathbf{e}_2 \otimes \mathbf{e}_2, \quad (2.8)$$

where α_i ($i = 1, 2$) represent the elastic principal stretches, and g_i are growth factors. There is no volume change in the i -direction when $g_i = 1$, and $g_i > 1$, $g_i < 1$ represent growth and shrinkage, respectively. In this work, we only consider volume increase, meaning that the growth factors are always greater than unity. Since the deformation in the X_1 -direction is limited so that $\lambda_1 = 1$, we have $\alpha_1 = g_1^{-1}$. Further, according to the elastic incompressibility condition $\det \mathbf{A} = 1$, we have $\alpha_1 \alpha_2 = 1$ and hence $\alpha_2 = g_1$ and $\lambda_2 = g_1 g_2$. Here we denote the strain–energy function by $W = W(\mathbf{A})$ (or $W = W(\alpha_1, \alpha_2)$), and an explicit expression of the Cauchy stress (2.4) is given by Goriely (2017):

$$\sigma = \mathbf{A} \frac{\partial W}{\partial \mathbf{A}} - p\mathbf{I}. \quad (2.9)$$

According to the equilibrium equation (2.5), the traction-free boundary condition on $x_2 = 0$, and the traction continuity condition on the interface $x_2 = h$, we find

$$\hat{p} = \hat{g}_1 \hat{W}_2, \quad p = g_1 W_2, \quad (2.10)$$

where $W_2 = \partial W / \partial \alpha_2$.

2.3. Incremental theory

Next, we are interested in the possible existence of some states B_i close to B_r . We obtain them by superimposing an infinitesimal displacement field $\mathbf{u}(\mathbf{x}) = u_1(x_1, x_2)\mathbf{e}_1 + u_2(x_1, x_2)\mathbf{e}_2$ on B_r . In this way, the position vector of a material particle relative to the common orthonormal basis is denoted by $\tilde{\mathbf{x}}$, which satisfies the following relation

$$\tilde{\mathbf{x}}(\mathbf{X}) = \mathbf{x}(\mathbf{X}) + \mathbf{u}(\mathbf{x}). \quad (2.11)$$

The deformation gradient arising from $B_0 \rightarrow B_i$ is $\tilde{\mathbf{F}} = \partial \tilde{\mathbf{x}} / \partial \mathbf{X} = (\mathbf{I} + \boldsymbol{\eta})\mathbf{F}$, with

$$\boldsymbol{\eta} = \frac{\partial u_i}{\partial x_j} \mathbf{e}_i \otimes \mathbf{e}_j \equiv u_{i,j} \mathbf{e}_i \otimes \mathbf{e}_j, \quad (2.12)$$

where repeated indices imply a summation from 1 to 2. The linearized incompressibility constraint then reads

$$\text{tr } \boldsymbol{\eta} = u_{i,i} = 0, \quad (2.13)$$

where ‘tr’ is the trace operator.

The first Piola–Kirchhoff stress tensors in B_r and B_i are denoted by $\boldsymbol{\pi}$ and $\tilde{\boldsymbol{\pi}}$, respectively. It is convenient to introduce the incremental stress tensor χ by

$$\chi = J^{-1}(\tilde{\boldsymbol{\pi}} - \boldsymbol{\pi})\mathbf{F}^T, \quad (2.14)$$

where $J = \det \mathbf{F}$ and ‘T’ is the transpose. The incremental equations for the substrate in terms of χ are

$$\text{div } \chi^T = \mathbf{0}, \quad (2.15)$$

and, similarly, for the film:

$$\operatorname{div} \hat{\chi}^T = \mathbf{0}. \quad (2.16)$$

The incremental boundary condition and continuity condition are:

(i) the traction-free boundary condition,

$$\hat{\chi} \mathbf{e}_2 = \mathbf{0}, \quad \text{on } x_2 = 0; \quad (2.17)$$

(ii) the continuity condition,

$$(\chi - \hat{\chi}) \mathbf{e}_2 = \mathbf{0}, \quad \mathbf{u} - \hat{\mathbf{u}} = \mathbf{0}, \quad \text{on } x_2 = h; \quad (2.18)$$

(iii) the decay condition,

$$\mathbf{u} = \mathbf{0}, \quad \text{as } x_2 \rightarrow \infty; \quad (2.19)$$

(iv) the sliding-end condition,

$$\chi \mathbf{e}_1 = \mathbf{0}, \quad \hat{\chi} \mathbf{e}_1 = \mathbf{0}, \quad u_{1,2} = 0, \quad \hat{u}_{1,2} = 0, \quad \text{on } x_1 = 0 \text{ and } l. \quad (2.20)$$

For an incremental deformation, the magnitude of η is small and we can therefore expand χ in η and retain the linear terms to obtain

$$\chi_{ij} = \mathcal{A}_{jilk} \eta_{kl} + p \eta_{ji} - \dot{p} \delta_{ji} + \mathcal{O}(|\eta_{ij}|^2), \quad (2.21)$$

where the pressure p has been defined in (2.4), \dot{p} is the incremental counterpart, and the fourth-order tensor \mathcal{A} defines instantaneous moduli whose components are given by

$$\mathcal{A}_{jilk} = F_{jA} F_{lB} \frac{\partial^2 W}{\partial \tilde{F}_{iA} \partial \tilde{F}_{kB}} \bigg|_{\tilde{\mathbf{F}}=\mathbf{F}}, \quad \text{in the compression case,} \quad (2.22)$$

$$\mathcal{A}_{jilk} = A_{jA} A_{lB} \frac{\partial^2 W}{\partial \tilde{A}_{iA} \partial \tilde{A}_{kB}} \bigg|_{\tilde{\mathbf{A}}=\mathbf{A}}, \quad \text{in the growth case.} \quad (2.23)$$

The set of Eqs. (2.15)–(2.20) with the incompressibility constraints for both layers form a linear system for which we seek solutions. More precisely, we are interested in finding values of the parameter (either compression or growth), such that there exists a non-trivial solution to this system. These values are the critical values for the bifurcation.

3. Bifurcation analysis

We will apply the Stroh method (Stroh, 1962; Fu and Mielke, 2002; Fu, 2005; Su et al., 2016, 2019; Su, 2020; Liu et al., 2022) and the surface impedance matrix method (Biryukov, 1985; Biryukov et al., 1995; Shuvalov, 2003b,a) to obtain the critical buckling load and its associated wavenumber rather than the determinant method or the compound matrix method (Jin et al., 2018; Liu, 2018).

3.1. Stroh formulation and the surface impedance matrix method

To describe the initial wrinkling pattern, we look for a solution of the form

$$u_1(x_1, x_2) = U(x_2) \sin(nx_1), \quad u_2(x_1, x_2) = V(x_2) \cos(nx_1), \quad \dot{p}(x_1, x_2) = P(x_2) \cos(nx_1), \quad (3.1)$$

where $U(x_2)$, $V(x_2)$ and $P(x_2)$ are unknown functions to be determined and n is the wavenumber. Note that in the current problem the same n is used for both the substrate and the film. It then follows from the sliding end condition (2.20) that

$$n = \frac{k\pi}{l}, \quad (3.2)$$

where k is the dimensionless wavenumber and $l = \lambda L$. Remember that in the growth case the principal stretch λ is always unity.

The components of the incremental stress tensor χ can be expressed as

$$\chi_{12}(x_1, x_2) = T_{12}(x_2) \sin(nx_1), \quad \chi_{22}(x_1, x_2) = T_{22}(x_2) \cos(nx_1), \quad (3.3)$$

where $T_{12}(x_2)$ and $T_{22}(x_2)$ are unknown functions.

To simplify book-keeping, we scale all coordinates and variables of length dimension by L . In addition, all variables of the stress unit are normalized by μ_h . Here L is the length of the bilayer and μ_h is the shear modulus on the substrate surface ($X_2 = h_0$). This yields

$$\begin{aligned} x &= \frac{x_1}{L}, \quad y = \frac{x_2}{L}, \quad X = \frac{X_1}{L}, \quad Y = \frac{X_2}{L}, \quad U^* = \frac{U}{L}, \quad V^* = \frac{V}{L}, \quad h_0^* = \frac{h_0}{L}, \quad h^* = \frac{h}{L}, \\ p^* &= \frac{p}{\mu_h}, \quad P^* = \frac{P}{\mu_h}, \quad \mathcal{A}_{jilk}^* = \frac{\mathcal{A}_{jilk}}{\mu_h}, \quad T_{12}^* = \frac{T_{12}}{\mu_h}, \quad T_{22}^* = \frac{T_{22}}{\mu_h}, \quad \hat{\mathcal{A}}_{jilk}^* = \frac{\hat{\mathcal{A}}_{jilk}}{\mu_h}, \quad \gamma = \frac{\hat{\mu}}{\mu_h}, \end{aligned} \quad (3.4)$$

where $\hat{\mu}$ is the uniform ground state shear modulus for the film and γ measures the modulus ratio between the film and the substrate surface. To further simplify notations, we drop the asterisk from now on. The same nondimensionalization procedure will be applied to the film as well and we omit details.

We obtain relationship between $U(y)$ and $V(y)$ from the linearized incompressibility condition (2.13):

$$\frac{k\pi}{\lambda} U(y) + V'(y) = 0, \quad (3.5)$$

where a prime denotes a derivative with respect to y . Similarly, $P(y)$ can be solved from the expression of χ_{22} :

$$P(y) = \frac{k\pi}{\lambda} (\mathcal{A}_{2211} - \mathcal{A}_{2222} - p) U(y) - T_{22}(y). \quad (3.6)$$

Next, we define the displacement vector $\mathbf{u}(y) = [U(y), V(y)]^T$ (the incremental displacement with dimension has been used in (2.11)), the traction vector $\mathbf{T}(y) = [T_{12}(y), T_{22}(y)]^T$, and write their combination as a displacement-traction vector

$$\xi(y) = [\mathbf{u}(y), \mathbf{T}(y)]^T. \quad (3.7)$$

Based on the Eqs. (2.15), (2.21), (3.5) and (3.6) we recast the boundary-value problem given by (2.15)–(2.20) as a differential equation for the displacement-traction vector:

$$\xi'(y) = \mathbf{Q}(y)\xi(y). \quad (3.8)$$

This way of posing the problem is known as the *Stroh formulation* of the implied incremental problem (Stroh, 1962; Fu, 2005), where $\mathbf{Q}(y)$ is the Stroh matrix possessing the following block formulation:

$$\mathbf{Q}(y) = \begin{bmatrix} \mathbf{Q}_1 & \mathbf{Q}_2 \\ \mathbf{Q}_3 & \mathbf{Q}_4 \end{bmatrix}, \quad (3.9)$$

and \mathbf{Q}_i ($i = 1, 2, 3, 4$) are 2×2 sub-blocks such that \mathbf{Q}_2 and \mathbf{Q}_3 are real symmetric, and $\mathbf{Q}_4 = -\mathbf{Q}_1^T$. In particular, the matrices \mathbf{Q}_1 , \mathbf{Q}_2 and \mathbf{Q}_3 are given by

$$\begin{aligned} \mathbf{Q}_1 &= \frac{k\pi}{\lambda} \begin{bmatrix} 0 & \frac{\mathcal{A}_{2112} + p}{\mathcal{A}_{2121}} \\ -1 & 0 \end{bmatrix}, \quad \mathbf{Q}_2 = \begin{bmatrix} \frac{1}{\mathcal{A}_{2121}} & 0 \\ 0 & 0 \end{bmatrix}, \\ \mathbf{Q}_3 &= \left(\frac{k\pi}{\lambda}\right)^2 \begin{bmatrix} \mathcal{A}_{1111} - \mathcal{A}_{2211} + \mathcal{A}_{2222} + 2p & 0 \\ 0 & \mathcal{A}_{1212} - \frac{(\mathcal{A}_{1221} + p)^2}{\mathcal{A}_{2121}} \end{bmatrix}. \end{aligned} \quad (3.10)$$

Note that in obtaining the expression of \mathbf{Q}_3 we have used the fact that $\mathcal{A}_{2112} = \mathcal{A}_{1221}$.

We apply the *impedance matrix method* (Biryukov, 1985; Biryukov et al., 1995; Shuvalov, 2003b,a) to solve the incremental problem. To this end, we first assume a relation between the displacement vector $\mathbf{u}(y)$ and traction vector $\mathbf{T}(y)$:

$$\mathbf{u}(y) = \mathbf{K}(y)\mathbf{T}(y), \quad (3.11)$$

with $\mathbf{K}(y)$ an unknown matrix. It can be derived from the decay displacement boundary condition $\mathbf{u}(\infty) = \mathbf{0}$ that $\mathbf{K}(\infty) = \mathbf{0}$. Now substituting Eqs. (3.7) and (3.11) into (3.8) and eliminating the dependence of $\mathbf{T}(y)$, we obtain a *Riccati equation* for \mathbf{K} :

$$\mathbf{K}' = \mathbf{Q}_2 - \mathbf{K}\mathbf{Q}_4 - \mathbf{K}\mathbf{Q}_3\mathbf{K} + \mathbf{Q}_1\mathbf{K}, \quad h < y < \infty. \quad (3.12)$$

For the film with a free lateral boundary, instead of Eq. (3.11), we use as an ansatz a different relation between $\hat{\mathbf{u}}(y)$ and $\hat{\mathbf{T}}(y)$, which is written as

$$\hat{\mathbf{T}}(y) = \mathbf{Z}(y)\hat{\mathbf{u}}(y), \quad (3.13)$$

where $\mathbf{Z}(y)$ is known as the *surface impedance matrix*. It follows from the traction-free boundary condition $\hat{\mathbf{T}}(0) = \mathbf{0}$ that $\mathbf{Z}(0) = \mathbf{0}$.

For the substrate, we obtain the following differential matrix *Riccati equation* by applying a similar derivation procedure:

$$\mathbf{Z}' = \hat{\mathbf{Q}}_3 - \mathbf{Z}\hat{\mathbf{Q}}_1 - \mathbf{Z}\hat{\mathbf{Q}}_2\mathbf{Z} + \hat{\mathbf{Q}}_4\mathbf{Z}, \quad 0 < y < h. \quad (3.14)$$

The expressions of $\hat{\mathbf{Q}}_i$ ($i = 1, 2, 3, 4$) are determined from (3.10) by suitable variable substitutions.

We can solve numerically the Eq. (3.12) subject to the boundary condition $\mathbf{K}(\infty) = \mathbf{0}$. In this way, the traction on the interface is given by $\mathbf{T}(h) = \mathbf{K}^{-1}(h)\mathbf{u}(h)$. Meanwhile, a similar solution procedure for Eq. (3.14) can be applied and as a result the traction on the interface is written as $\mathbf{Z}(h)\hat{\mathbf{u}}(h)$. The continuity condition gives $(\mathbf{Z}(h) - \mathbf{K}^{-1}(h))\mathbf{u}(h) = \mathbf{0}$. The existence of a non-trivial solution of $\mathbf{u}(h)$ then requires

$$\det(\mathbf{Z}(h)\mathbf{K}(h) - \mathbf{I}) = 0, \quad (3.15)$$

which is the bifurcation condition. This bifurcation condition (3.15) is valid for both problems considered in this study. Once the strain–energy function and the shear modulus distribution function are specified, one can obtain the onset of surface wrinkling by solving (3.15) numerically.

3.2. Preliminary for asymptotic analysis

In this subsection, we return to the original incremental equations and transform it into an equivalent fourth-order ordinary differential equation suitable for asymptotic analysis. For that purpose, we substitute (2.21), (3.1) into the governing system (2.13), (2.15) and eliminate all unknowns except for $V(y)$. Ultimately, we acquire a dimensionless fourth-order ODE for $V(y)$ by utilizing the dimensionless variables in (3.4), which takes the following form

$$\begin{aligned} V'''' + \frac{2\mathcal{A}'_{2121}}{\mathcal{A}_{2121}} V''' + \frac{k^2\pi^2}{\lambda^2\mathcal{A}_{2121}} (\mathcal{A}_{1122} - \mathcal{A}_{1111} + 2\mathcal{A}_{1221} + \mathcal{A}_{2211} - \mathcal{A}_{2222}) + \frac{\mathcal{A}''_{2121}}{\mathcal{A}_{2121}} V'' \\ + \frac{k^2\pi^2}{\lambda^2\mathcal{A}_{2121}} (\mathcal{A}'_{1122} - \mathcal{A}'_{1111} + 2\mathcal{A}'_{1221} + \mathcal{A}'_{2211} - \mathcal{A}'_{2222}) V' \\ + \frac{k^2\pi^2}{\lambda^2\mathcal{A}_{2121}} \left(\frac{k^2\pi^2}{\lambda^2} \mathcal{A}_{1212} + p'' + \mathcal{A}''_{2112} \right) V = 0. \end{aligned} \quad (3.16)$$

Moreover, the traction components are given by

$$T_{12} = \mathcal{A}_{2121} V'' + \frac{k^2\pi^2}{\lambda^2} (p + \mathcal{A}_{2112}) V, \quad (3.17)$$

$$\begin{aligned} T_{22} = \mathcal{A}_{2121} V''' + \mathcal{A}'_{2121} V'' - \frac{k^2\pi^2}{\lambda^2} (p + \mathcal{A}_{1111} - 2\mathcal{A}_{1122} - \mathcal{A}_{2112} + \mathcal{A}_{2222}) V' \\ + \frac{k^2\pi^2}{\lambda^2} (p' + \mathcal{A}'_{2112}) V, \end{aligned} \quad (3.18)$$

and the boundary conditions and continuity conditions (2.17)–(2.19) are transformed into

$$\begin{aligned} \hat{T}_{12} = 0, \quad \hat{T}_{22} = 0, \quad \text{on } y = 0, \\ \hat{T}_{12} = T_{12}, \quad \hat{T}_{22} = T_{22}, \quad \hat{V} = V, \quad \hat{V}' = V', \quad \text{on } y = h, \\ V = 0, \quad V' = 0, \quad \text{as } y \rightarrow \infty. \end{aligned} \quad (3.19)$$

This formulation is valid for both the compression and the growth cases.

4. WKB reduction

We consider the short wavelength approximation, i.e. $k \rightarrow \infty$, to carry out an asymptotic analysis on the critical condition of surface wrinkling, following Jin et al. (2018).

First, to make progress we must choose a material model. Here, we will use the neo-Hookean model but other choices can be used within the same setting. Note that an asymptotic formula for the critical buckling stretch has been derived by Cai and Fu (1999) when the substrate is homogeneous and the incompressible neo-Hookean model is employed. This will be used as a benchmark for validating the asymptotic solutions in our particular situation. In the plane-strain case, the strain-energy functions for the film and substrate are given by

$$\hat{W} = \frac{1}{2} \hat{\mu} (I_1 - 2), \quad W = \frac{1}{2} \mu_s(X_2) (I_1 - 2), \quad (4.1)$$

where $\hat{\mu}$ is the homogeneous ground state shear modulus of the film, $\mu_s(X_2)$ is the modulus function, and $I_1 = \text{tr } \mathbf{FF}^T$ if the external load is given by axial compression or $I_1 = \text{tr } \mathbf{AA}^T$ in the growth case. Before proceeding further, we introduce the dimensionless modulus

$$\mu(y) = \frac{\mu_s}{\mu_h}, \quad (4.2)$$

where μ_h has been defined in (3.4).

4.1. Uniaxial compression

For the neo-Hookean model (4.1), the fourth-order ODE (3.16) simplifies to

$$V'''' + \frac{2\mu'}{\mu} V''' + \left(\frac{\mu''}{\mu} - \frac{k^2\pi^2(\lambda^4 + 1)}{\lambda^2} \right) V'' - \frac{k^2\pi^2(\lambda^4 + 1)\mu'}{\lambda^2\mu} V' + k^2\pi^2 \left(\frac{\mu''}{\lambda^2\mu} + k^2\pi^2 \right) V = 0. \quad (4.3)$$

The boundary conditions and continuity conditions in (3.19) become

$$\begin{aligned} \hat{V}''' - \frac{k^2\pi^2(\lambda^4 + 2)}{\lambda^2} \hat{V}' = 0, \quad \hat{V}'' + \frac{k^2\pi^2}{\lambda^2} \hat{V} = 0, \quad \text{on } y = 0, \\ \gamma \hat{V}''' - \mu V''' - \mu' V'' - \frac{\gamma k^2\pi^2(\lambda^4 + 2)}{\lambda^2} \hat{V}' + \frac{k^2\pi^2(\lambda^4 + 2)\mu}{\lambda^2} V' - \frac{k^2\pi^2\mu'}{\lambda^2} V = 0, \quad \text{on } y = h, \\ \gamma \hat{V}'' - \mu V'' + \gamma \frac{k^2\pi^2}{\lambda^2} \hat{V} - \frac{k^2\pi^2\mu}{\lambda^2} V = 0, \quad \text{on } y = h, \\ \hat{V} - V = 0, \quad \hat{V}' - V' = 0, \quad \text{on } y = h, \\ V = 0, \quad V' = 0, \quad \text{as } y \rightarrow \infty. \end{aligned} \quad (4.4)$$

The above equation (4.3) is for the substrate; its counterpart for the film can be found by replacing V by \hat{V} and by setting all derivative terms of μ to zero as the film is composed of a homogeneous material. Accordingly, the fourth-order ODE for the film is given by

$$\hat{V}'''' - \frac{k^2\pi^2(\lambda^4 + 1)}{\lambda^2}\hat{V}'' + k^4\pi^4\hat{V} = 0. \quad (4.5)$$

Solving directly the associated characteristic equation yields four eigenvalues $s_{1,2} = \mp k\pi/\lambda$ and $s_{3,4} = \mp k\pi\lambda$. Correspondingly, the general solution to Eq. (4.5) can be written as

$$\hat{V}(y) = C_1 \exp(s_1 y) + C_2 \exp(s_2 y) + C_3 \exp(s_3 y) + C_4 \exp(s_4 y), \quad (4.6)$$

where C_i ($i = 1, 2, 3, 4$) are constants.

Following the WKB method, we seek for a solution of (4.3) by using the following ansatz (Hinch, 1991)

$$V(y) = \exp\left(\int_y^\infty S(\tau) d\tau\right). \quad (4.7)$$

Substituting the solution (4.7) into (4.3) gives

$$\begin{aligned} S^4 - \frac{2\mu'}{\mu}(S^3 + S'' - 3SS') - 6S^2S' + 4SS'' + 3S'^2 - S''' + \left(\frac{\mu''}{\mu} - \frac{k^2\pi^2(\lambda^4 + 1)}{\lambda^2}\right)(S^2 - S') \\ + \frac{k^2\pi^2(\lambda^4 + 1)\mu'}{\lambda^2\mu}S + k^4\pi^4 + \frac{k^2\pi^2\mu''}{\lambda^2\mu} = 0. \end{aligned} \quad (4.8)$$

The next step is to look for an asymptotic solution to the above equation of the form

$$S(y) = kS_0 + S_1 + k^{-1}S_2 + \dots = \sum_{m=0}^{\infty} k^{1-m}S_m, \quad (4.9)$$

where S_m ($m = 0, 1, 2, \dots$) are unknown functions of y . Substituting (4.9) into (4.8) and equating all coefficients of like powers of $1/k$ to zero provide infinitely many equations. In particular, the leading-order equation is a quartic algebraic one of S_0 from which four independent solutions can be obtained. Typically, a two-term approximation containing S_0 and S_1 in (4.9) already provides sufficient accuracy (Jin et al., 2018). The four independent solutions for $S(y)$ are:

$$S^{(1,2)}(y) = \mp \frac{k\pi}{\lambda} + \frac{\mu'}{2\mu} + \dots, \quad S^{(3,4)}(y) = \mp k\pi\lambda + \frac{\mu'}{2\mu} + \dots. \quad (4.10)$$

Then, the general solution for $V(y)$ can be written as

$$V(y) = \sum_{i=1}^4 C_{i+4} \exp\left(\int_y^\infty S^{(i)}(\tau) d\tau\right), \quad (4.11)$$

where C_{i+4} ($i = 1, 2, 3, 4$) are arbitrary constants. Inserting (4.6) and (4.11) into (4.4), we obtain a vector equation

$$\mathbf{M}\mathbf{C} = \mathbf{0}, \quad (4.12)$$

where $\mathbf{C} = [C_1, C_2, C_3, C_4, C_5, C_6, C_7, C_8]^T$ and the coefficient matrix \mathbf{M} is given by

$$\mathbf{M} = \begin{bmatrix} \hat{a}_1 & \hat{a}_2 & \hat{a}_3 & \hat{a}_4 & 0 & 0 & 0 & 0 \\ \hat{b}_1 & \hat{b}_2 & \hat{b}_3 & \hat{b}_4 & 0 & 0 & 0 & 0 \\ q_1\hat{a}_1 & q_2\hat{a}_2 & q_3\hat{a}_3 & q_4\hat{a}_4 & f_1a_1 & f_2a_2 & f_3a_3 & f_4a_4 \\ q_1\hat{b}_1 & q_2\hat{b}_2 & q_3\hat{b}_3 & q_4\hat{b}_4 & f_1b_1 & f_2b_2 & f_3b_3 & f_4b_4 \\ q_1 & q_2 & q_3 & q_4 & -f_1 & -f_2 & -f_3 & -f_4 \\ q_1s_1 & q_2s_2 & q_3s_3 & q_4s_4 & f_1S^{(1)}(h) & f_2S^{(2)}(h) & f_3S^{(3)}(h) & f_4S^{(4)}(h) \\ 0 & 0 & 0 & 0 & 1 & 1 & 1 & 1 \\ 0 & 0 & 0 & 0 & -S^{(1)}(\infty) & -S^{(2)}(\infty) & -S^{(3)}(\infty) & -S^{(4)}(\infty) \end{bmatrix}. \quad (4.13)$$

Note that the parameters $\hat{a}_i, \hat{b}_i, a_i, b_i, q_i$, and f_i are defined as

$$\begin{aligned} \hat{a}_i &= \gamma s_i \left(s_i^2 - \frac{k^2\pi^2(\lambda^4 + 2)}{\lambda^2} \right), \quad \hat{b}_i = \gamma \left(s_i^2 + \frac{k^2\pi^2}{\lambda^2} \right), \quad q_i = \exp(s_i h), \\ a_i &= S^{(i)}(h)^3 \mu(h) - S^{(i)}(h)^2 \mu'(h) - S^{(i)}(h) \mu(h) \left(3S^{(i)'}(h) + \frac{k^2\pi^2}{\lambda^2}(\lambda^4 + 2) \right) \\ &\quad + S^{(i)''}(h) \mu(h) + \left(S^{(i)'}(h) - \frac{k^2\pi^2}{\lambda^2} \right) \mu'(h), \\ b_i &= \mu(h) \left(S^{(i)'}(h) - S^{(i)}(h)^2 - \frac{k^2\pi^2}{\lambda^2} \right), \quad f_i = \exp\left(\int_h^\infty S^{(i)}(\tau) d\tau\right). \end{aligned} \quad (4.14)$$

The existence of a non-trivial solution to (4.12) requests the vanishing of the determinant of \mathbf{M} . Finally, the bifurcation condition reads

$$\det \mathbf{M} = 0, \quad (4.15)$$

which can be regarded as a function of the principal stretch λ , the wavenumber k , the modulus ratio γ , the thickness h_0 and the parameters involved in the modulus function $\mu(y)$. After a careful observation of the coefficients in (4.14), we find that f_2 and f_4 are both exponentially large so the terms whose factor is $f_2 f_4$ will dominate the value of determinant. As a result, the bifurcation condition (4.15) can be rewritten as

$$\Xi = \frac{\det \mathbf{M}}{f_2 f_4} - E.S.T. = 0, \quad (4.16)$$

where $E.S.T$ denotes exponential small terms which will be neglected in further analysis and the algebraic equation $\Xi = 0$ provides a way to obtain an analytical formula for the critical bifurcation threshold.

4.2. Restricted growth

When the compressive stress is induced by growth, the bifurcation parameter is the growth factor. The strain–energy functions for the film and the substrate are provided by (4.1). In this case, the dimensionless fourth-order ODE (3.16) is

$$\begin{aligned} V''''(y) + \frac{2\mu'}{\mu} V''' + \left(\frac{\mu''}{\mu} - k^2 \pi^2 \left(\frac{1}{g_1^4} + 1 \right) \right) V'' - \frac{k^2 \pi^2 (g_1^4 + 1) \mu'}{g_1^4 \mu} V' \\ + \left(\frac{k^2 \pi^2 \mu''}{\mu} + \frac{k^4 \pi^4}{g_1^4} \right) V = 0, \end{aligned} \quad (4.17)$$

where g_1 is the growth factor for the substrate in the horizontal direction. Correspondingly, the incremental boundary conditions and continuity conditions in (3.19) can be written as

$$\begin{aligned} \hat{V}''' - k^2 \pi^2 \left(\frac{1}{\hat{g}_1^4} + 2 \right) \hat{V}' &= 0, \quad \hat{V}'' + k^2 \pi^2 \hat{V} = 0, \quad \text{on } y = 0, \\ \gamma \hat{g}_1^2 \hat{V}''' - g_1^2 \mu V''' - g_1^2 \mu' V'' - \frac{\gamma k^2 \pi^2 (2\hat{g}_1^4 + 1)}{\hat{g}_1^2} \hat{V}' + \frac{\mu k^2 \pi^2 (2g_1^4 + 1)}{g_1^2} V' - g_1^2 k^2 \pi^2 \mu' V &= 0, \quad \text{on } y = h, \\ \gamma \hat{g}_1^2 \hat{V}'' - g_1^2 \mu V'' + \gamma \hat{g}_1^2 k^2 \pi^2 \hat{V} - g_1^2 k^2 \pi^2 \mu V &= 0, \quad \text{on } y = h, \\ \hat{V} - V = 0, \quad \hat{V}' - V' = 0, \quad \text{on } y = h, \\ V = 0, \quad V' = 0, \quad \text{as } y \rightarrow \infty. \end{aligned} \quad (4.18)$$

In our previous study (Liu et al., 2021), it was found that a gradient in the growth function has a negligible effect on the critical buckling threshold and a constant growth can provide a good approximation on interpreting complicated morphological formations in bilayer systems. Thus, we assume that both layers share the same constant growth factor such that $\hat{g}_1 = \hat{g}_2 = g_1 = g_2 = g$. Next, we aim to solve asymptotically the eigenvalue problem with variable coefficients arising from (4.17) and (4.18).

The fourth-order ODE for the homogeneous film can be obtained by removing all derivative terms of the shear modulus in (4.17). Solving directly the associated characteristic equation gives a general solution of $\hat{V}(y)$ of the form

$$\hat{V}(y) = C_1 \exp(r_1 y) + C_2 \exp(r_2 y) + C_3 \exp(r_3 y) + C_4 \exp(r_4 y), \quad (4.19)$$

where C_i ($i = 1, 2, 3, 4$) are constants and the eigenvalues r_i ($i = 1, 2, 3, 4$) are given by $r_{1,2} = \mp k\pi$ and $r_{3,4} = \mp k\pi/g^2$.

To solve (4.17), we use again a WKB-type method with ansatz given by

$$V(y) = \exp \left(\int_y^\infty R(\tau) d\tau \right), \quad (4.20)$$

and the integrand function can be expanded in k as

$$R(y) = kR_0 + R_1 + k^{-1}R_2 + \dots = \sum_{m=0}^{\infty} k^{1-m} R_m, \quad (4.21)$$

where R_m ($m = 0, 1, 2, \dots$) are unknown functions of y . On substituting Eqs. (4.20) and (4.21) into (4.17) we also figure out four solutions of R_0 from the leading-order equation. Similar to the solution procedure illustrated in Section 4.1, we are able to obtain the following four independent solutions

$$R^{(1,2)}(y) = \mp k\pi + \frac{\mu'(y)}{2\mu(y)} + \dots, \quad R^{(3,4)}(y) = \mp \frac{k\pi}{g^2} + \frac{\mu'(y)}{2\mu(y)} + \dots. \quad (4.22)$$

The general form of $V(y)$ is

$$V(y) = \sum_{i=1}^4 C_{i+4} \exp \left(\int_y^\infty R^{(i)}(\tau) d\tau \right), \quad (4.23)$$

where C_{i+4} ($i = 1, 2, 3, 4$) are constants. We further substitute (4.19) and (4.23) into (4.18) to obtain a vector equation of the same form as (4.12) but with all $S^{(i)}$ and s_i in (4.13) replaced by $R^{(i)}$ and r_i , and entries given by

$$\begin{aligned} \hat{a}_i &= \gamma r_i (g^4 r_i^2 - k^2 \pi^2 (2g^4 + 1)), \quad \hat{b}_i = \gamma (r_i^2 + k^2 \pi^2), \quad q_i = \exp(r_i h), \\ a_i &= g^4 \left(R^{(i)}(h)^3 \mu(h) - R^{(i)}(h)^2 \mu'(h) R^{(i)''}(h) \mu(h) + \left(R^{(i)'}(h) - k^2 \pi^2 \right) \right. \\ &\quad \left. - R^{(i)}(h) \mu(h) \left(3g^4 R^{(i)'}(h) + k^2 \pi^2 (2g^4 + 1) \right) \right), \\ b_i &= \mu(h) \left(R^{(i)'}(h) - R^{(i)}(h)^2 - k^2 \pi^2 \right), \quad f_i = \exp \left(\int_h^\infty R^{(i)}(y) dy \right). \end{aligned} \quad (4.24)$$

As in the previous case, the WKB analysis generates an approximate bifurcation condition $\bar{\Xi} = 0$ from $\det \bar{\mathbf{M}} = 0$, which will be used later on.

4.3. The shear modulus various exponentially

The problem cannot be solved for an arbitrary modulus function. Hence, we consider a modulus with an exponential decay of the form

$$\mu_s(X_2) = \mu_0 \exp(-\zeta(X_2 - h_0)) + \mu_1, \quad X_2 \geq h_0, \quad \text{the original notations with dimension,} \quad (4.25)$$

where μ_0, μ_1 are two constants, and $\zeta > 0$ measures how fast the modulus decays ($\zeta > 0$ and $(\mu_0 + \mu_1)/\mu_1 > 1$) or grows (either $\zeta < 0$ or $\zeta > 0$ and $(\mu_0 + \mu_1)/\mu_1 < 1$) from the surface of substrate. If $\zeta > 0$, we find $\mu_0 + \mu_1 = \mu(h_0) = \mu_h$ and $\mu_1 = \mu(\infty) = \mu_\infty$, or otherwise we require $\mu_0 + \mu_1 = \mu_h$ and $\mu_\infty = \infty$. Then the dimensionless form of (4.25) with y as a variable reads

$$\mu(y) = (1 - \beta) \exp(-\alpha(\lambda y - h_0)) + \beta, \quad y \geq h, \quad (4.26)$$

where $\beta = \mu_\infty/\mu_h$ and $\alpha = \zeta L$ is the normalized decay rate. We also impose $\mu_1 \neq 0$ to avoid zero modulus (Chen et al., 2017). Using (4.26), we are able to express the bifurcation condition (4.16) as $\Xi(\lambda, k, \alpha, \beta, \gamma, h_0) = 0$. For the growth scenario, the exponential modulus function (4.26) is used as well but we substitute $\lambda = 1/g^2$ to obtain a condition in terms of g of the form $\bar{\Xi} = \bar{\Xi}(g, k, \alpha, \beta, \gamma, h_0) = 0$.

A particularly interesting situation arises when the substrate is more compliant than the thin film with γ large and h_0 small considered in Cao et al. (2012) and Chen et al. (2017). Our study unifies and generalizes both works by considering the two cases $\beta \sim \mathcal{O}(1)$ or small and large β .

5. Asymptotic solution when β is small or of $\mathcal{O}(1)$

We focus on $\beta \ll 1$ or $\beta \sim \mathcal{O}(1)$ and derive some asymptotic estimates for the critical buckling load as well as for the critical wavenumber. The compression and growth cases will be explored separately.

5.1. Uniaxial compression

Before carrying out the asymptotic analysis, we first present five bifurcation curves according to the exact bifurcation condition (3.15) in Fig. 2 when the modulus ratio $\gamma = 100$ and the initial film thickness $h_0 = 0.015$. The purpose is to identify some valid parameter domains where the short wavelength assumption can be satisfied. In Fig. 2 we see that each curve has a maximum, highlighted by a blue point; its vertical coordinate gives the critical stretch λ_{cr} triggering surface wrinkling while the horizontal coordinate gives the critical wavenumber k_{cr} . When $\alpha = 5$ or $\alpha = 10$ the critical wavenumber k_{cr} is unity, which does not satisfy the short wavelength assumption in the WKB expansion (4.9). Hence, we consider the case where $\alpha \sim \mathcal{O}(1)$. We also note that the specific value of β when $\beta \sim \mathcal{O}(1)$ or small has a weak effect on the critical state when the modulus ratio γ is large.

Next, we explore the influence of the film initial thickness h_0 on the critical state. Given $\gamma = 100$, $\alpha = 1$, $\beta = 0.01$, Fig. 3 shows nine bifurcation curves stemming from (3.15) for different values of h_0 . The dashed line is the envelope of the maximums of bifurcation curves. We observe that the critical wavenumber k_{cr} is a decreasing function of h_0 . To satisfy the short wavelength assumption, we confine our attention to small h_0 as found in many engineering devices or biological tissues. It is worth noting that λ_{cr} is independent of h_0 when the substrate is homogeneous (Cai and Fu, 1999; Liu and Dai, 2014; Alawiye et al., 2019; Wang et al., 2023), but in our problem λ_{cr} is no longer a constant as shown in Fig. 3. In addition, we assume that the film is much stiffer than the substrate, which implies that γ is large. It is also known that $\varepsilon = 1 - \lambda_{cr}$ is small as the film is much stiffer than the substrate. In conclusion, we will place ourselves in the situation where the following four parameters are small: $1/k, h_0, 1/\gamma$ and ε .

In Fig. 4, we compare the bifurcation curves based on the approximate bifurcation condition (4.16) (dashed line) and the exact one (3.15) (solid line) if $10 \leq \gamma \leq 500$ and $h_0 = 0.015, \alpha = 1, \beta = 0.01$. It can be seen that the asymptotic result is in good agreement with the exact (numerical) one for all cases, even when $k_{cr} = 3$. Similarly, we checked that the asymptotic bifurcation condition (4.16) remains valid when $\alpha \sim \mathcal{O}(1)$, $1/k, h_0, \varepsilon$, and $1/\gamma$ are all small parameters. Therefore, we can now start from this approximation (4.16) to obtain explicit solution for λ_{cr} and k_{cr} .

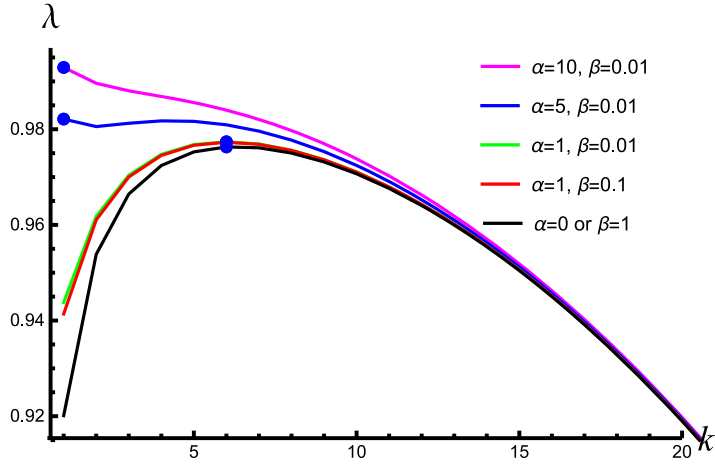


Fig. 2. Bifurcation curves based on the exact bifurcation condition (3.15) for $\gamma = 100$, $h_0 = 0.015$. The blue dots determine the critical principal stretch λ_{cr} associated with the critical wavenumber k_{cr} .

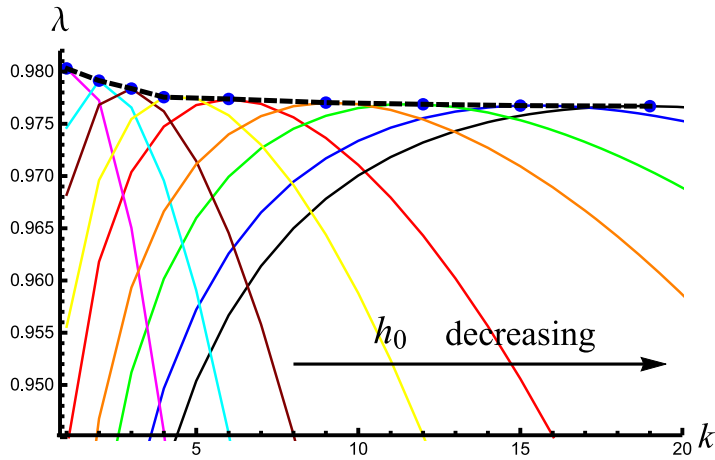


Fig. 3. Bifurcation curves based on the exact bifurcation condition (3.15) for $\gamma = 100$, $\alpha = 1$, $\beta = 0.01$ and $h_0 = 0.06, 0.04, 0.03, 0.02, 0.015, 0.01, 0.008, 0.006, 0.005$, respectively. Dashed line is the envelope of the bifurcation curves.

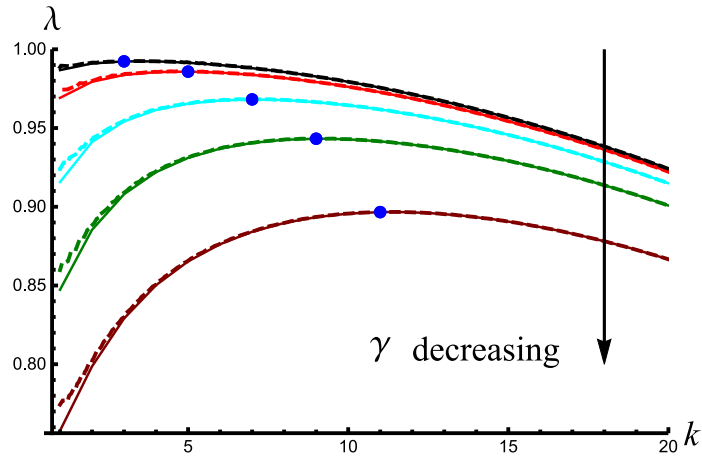


Fig. 4. Comparisons of the bifurcation curves between the approximate (dashed line) and exact (solid line) bifurcation conditions when $\gamma = 500, 200, 60, 25, 10$ and $h_0 = 0.015, \alpha = 1, \beta = 0.01$. The blue dots highlight the maximum that corresponds to the critical principal stretch λ_{cr} associated with the critical wavenumber k_{cr} .

5.1.1. Very stiff film on soft graded substrate: $\gamma \sim \mathcal{O}(h_0^{-\frac{3}{2}})$

First, we expand Eq. (4.16) in terms of the small parameters ε and h_0 to obtain

$$\begin{aligned} \varepsilon^2 & \left(t_0 k^4 + t_1 k^3 + t_2 k^5 h_0 + t_3 k^4 h_0 + t_4 k^6 h_0^2 + t_5 k^5 h_0^2 + \dots + \gamma (t_6 k^5 h_0 + t_7 k^4 h_0 \right. \\ & \left. + t_8 k^6 h_0^2 + t_9 k^5 h_0^2 + \dots) + \gamma^2 (t_{10} k^8 h_0^4 + t_{11} k^9 h_0^5) + \dots \right) + \varepsilon^3 \left(t_{12} k^4 + t_{13} k^3 \right. \\ & \left. + t_{14} k^5 h_0 + t_{15} k^4 h_0 + t_{16} k^6 h_0^2 + t_{17} k^5 h_0^2 + \dots + \gamma (t_{18} k^5 h_0 + t_{19} k^4 h_0 + t_{20} k^6 h_0^2 \right. \\ & \left. + t_{21} k^5 h_0^2 + \dots) + \gamma^2 (t_{22} k^6 h_0^2 + t_{23} k^7 h_0^3 + t_{24} k^8 h_0^4) + \dots \right) = 0, \end{aligned} \quad (5.1)$$

where t_i ($i = 0, 1, 2, \dots$) are constant coefficients related to α and β , whose lengthy expressions are not written out for brevity. The leading-order balance and principle of least degeneracy (Liu and Dai, 2014) are used to derive the order relations among ε and kh_0 and γ . Keeping all possible leading-order terms, (5.1) can be written as

$$t_0 + \gamma (t_6 k h_0 + t_8 k^2 h_0^2) + \gamma^2 (t_{10} k^4 h_0^4 + t_{11} k^5 h_0^5) + \varepsilon \gamma^2 (t_{22} k^2 h_0^2 + t_{23} k^3 h_0^3) + I.H.O. = 0, \quad (5.2)$$

where $t_0 \sim \mathcal{O}(1)$ and $I.H.O.$ represents infinitesimal of higher order. Analyzing and discussing all possible balances following Jin et al. (2018) and Liu and Dai (2014), we find that when $\varepsilon \sim \mathcal{O}(\gamma^{-\frac{2}{3}})$ and $kh_0 \sim \mathcal{O}(\gamma^{-\frac{1}{3}})$, the leading terms in (5.1) are of $\mathcal{O}(\gamma^{\frac{2}{3}})$ and are given by $t_6 k h_0 \gamma$, $t_{10} k^4 h_0^4 \gamma^2$ and $t_{22} k^2 h_0^2 \varepsilon \gamma^2$. Then, we extract all possible second-order terms for Eq. (5.1) and write

$$\mathcal{O}(\gamma^{\frac{2}{3}}) + t_0 + \gamma (t_7 h_0 + t_8 k^2 h_0^2) + \gamma^2 (t_{11} k^5 h_0^5 + t_{23} k^3 h_0^3 \varepsilon) + I.H.O. = 0, \quad (5.3)$$

where the terms $t_8 k^2 h_0^2 \gamma$, $t_{11} k^5 h_0^5 \gamma^2$ and $t_{23} k^3 h_0^3 \varepsilon \gamma^2$ are all of order $\mathcal{O}(\gamma^{\frac{1}{3}})$. Using the assumption that γ is a large parameter, we find that $\mathcal{O}(\gamma^{\frac{1}{3}}) \gg t_0$ and the second-order must be equal to $\mathcal{O}(\gamma^{\frac{1}{3}})$. According to the least degeneracy principle, in order to keep the $t_7 h_0 \gamma$ term, we can determine $h_0 \sim \mathcal{O}(\gamma^{-\frac{2}{3}})$ and $k \sim \mathcal{O}(\gamma^{\frac{1}{3}})$. Through the above analysis, the order relations are clearly given by $\varepsilon \sim \mathcal{O}(\gamma^{-\frac{2}{3}})$, $h_0 \sim \mathcal{O}(\gamma^{-\frac{2}{3}})$ and $k \sim \mathcal{O}(\gamma^{\frac{1}{3}})$.

To derive an asymptotic solution for λ_{cr} and k_{cr} , in addition to the Eq. (5.1) we also need to compute $\partial \lambda / \partial k = 0$, or equivalently

$$\frac{\partial \Xi}{\partial k} = 0. \quad (5.4)$$

Making use of the order relations we use

$$h_0 = a_0 \gamma^{-\frac{2}{3}}, \quad (5.5)$$

where a_0 is a constant of $\mathcal{O}(1)$. We then seek an asymptotic solution for λ_{cr} and k_{cr} in the form of

$$\begin{aligned} \lambda_{cr} &= 1 - \varepsilon = 1 - m_0 \gamma^{-\frac{2}{3}} - m_1 \gamma^{-1} - m_2 \gamma^{-\frac{4}{3}} - m_3 \gamma^{-\frac{5}{3}} + \dots, \\ k_{cr} &= l_0 \gamma^{\frac{1}{3}} + l_1 + l_2 \gamma^{-\frac{1}{3}} + l_3 \gamma^{-\frac{2}{3}} + \dots, \end{aligned} \quad (5.6)$$

where m_i and l_i ($i = 0, 1, 2, \dots$) are coefficients to be determined.

Substituting (5.6) into (4.16) and (5.4) provides the four-term asymptotic solutions

$$\begin{aligned} \lambda_{cr} &= 1 - \frac{3^{2/3}}{4\gamma^{2/3}} - \frac{3^{1/3}\alpha(\beta-1)h_0}{4\gamma^{1/3}} + \frac{1}{480} \left(\frac{99 \cdot 3^{1/3}}{\gamma^{4/3}} + \frac{40 \cdot 3^{2/3}\alpha(\beta-1)h_0}{\gamma^{2/3}} + 100\alpha^2(\beta-1)^2 h_0^2 \right) \\ &\quad - \frac{1}{720} \left(\frac{90 \cdot 3^{2/3}}{\gamma^{5/3}} - \frac{189\alpha(\beta-1)h_0}{\gamma} + \frac{30 \cdot 3^{1/3}\alpha^2(\beta^2-3\beta+2)h_0^2}{\gamma^{1/3}} \right) \\ &\quad + 10 \cdot 3^{2/3}\alpha^3(10\beta^3-32\beta^2+33\beta-11)\gamma^{1/3}h_0^3 + \mathcal{O}(\gamma^{-2}), \end{aligned} \quad (5.7)$$

$$\begin{aligned} k_{cr} &= \frac{3^{1/3}}{\pi\gamma^{1/3}h_0} + \frac{\alpha(\beta-1)}{\pi} - \frac{1}{60\pi} \left(\frac{81}{\gamma h_0} + \frac{10 \cdot 3^{1/3}\alpha(\beta-1)}{\gamma^{1/3}} + 35 \cdot 3^{2/3}\alpha^2(\beta-1)^2 \gamma^{1/3}h_0 \right) \\ &\quad - \frac{\alpha(\beta-1)}{180\pi} \left(\frac{42 \cdot 3^{2/3}}{\gamma^{2/3}} - 30\alpha(2\beta-3)h_0 - 5 \cdot 3^{1/3}\alpha^2(61\beta^2-130\beta+65)\gamma^{2/3}h_0^2 \right) \\ &\quad + \mathcal{O}(\gamma^{-1}). \end{aligned} \quad (5.8)$$

As a check to our method, we recover the homogeneous case by taking $\alpha = 0$ or $\beta = 1$ to obtain

$$\lambda_{cr}^{\circ} = 1 - \frac{3^{2/3}}{4\gamma^{2/3}} + \frac{33 \cdot 3^{1/3}}{160\gamma^{4/3}} - \frac{3^{2/3}}{8\gamma^{5/3}} + \mathcal{O}(\gamma^{-2}), \quad (5.9)$$

$$k_{cr}^{\circ} = \frac{3^{1/3}}{\pi\gamma^{1/3}h_0} - \frac{27}{20\pi\gamma h_0} + \mathcal{O}(\gamma^{-1}), \quad (5.10)$$

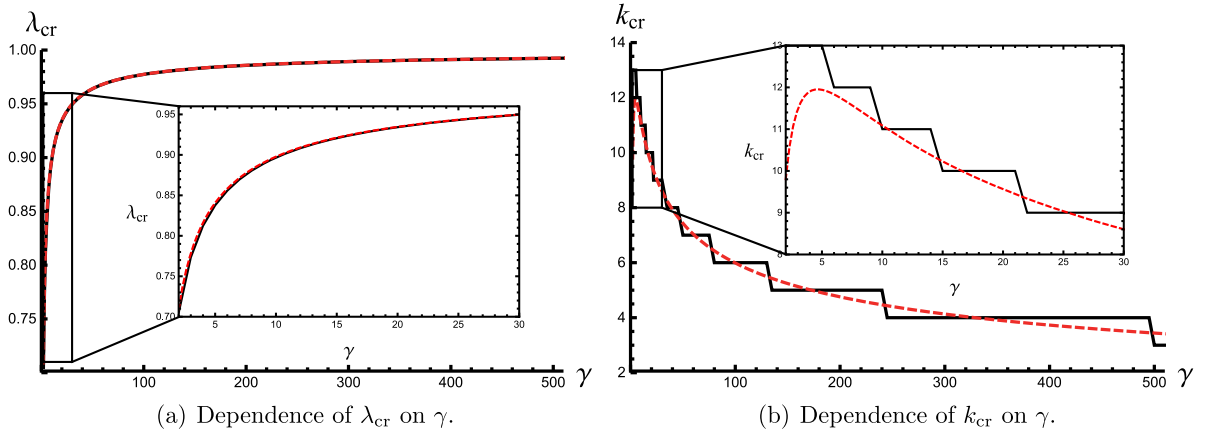


Fig. 5. Comparisons between the asymptotic (dashed line) and exact (solid line) solutions of λ_{cr} and k_{cr} for $h_0 = 0.015$, $\alpha = 1$, $\beta = 0.01$ when $\gamma \sim \mathcal{O}(h_0^{-\frac{3}{2}})$.

where an upper circle stands for the solution corresponding to a homogeneous substrate. Using (3.2) the estimate (5.10) gives

$$(nh_0)_{cr} = \frac{3^{1/3}}{\gamma^{1/3}} - \frac{3}{5\gamma} + \mathcal{O}(\gamma^{-5/3}) \quad \text{or} \quad (nh)_{cr} = \frac{3^{1/3}}{\gamma^{1/3}} + \frac{3}{20\gamma} + \mathcal{O}(\gamma^{-5/3}), \quad (5.11)$$

which is an exact match to the results found in Cai and Fu (1999), Alawiye et al. (2019) and Wang et al. (2023) up to $\mathcal{O}(\gamma^{-\frac{5}{3}})$.

A remarkable property of the solutions (5.7) and (5.8) is that all parameters relevant to gradients (given by α and β), only appear in higher order terms. In other words, it is the modulus ratio between the film and the substrate surface that dominates the critical bifurcation condition, and we find that the modulus gradient has a minor influence on λ_{cr} and k_{cr} . To further unravel how the modulus gradient affects the critical state, we define

$$\delta_1 = \overset{\circ}{\lambda}_{cr} - \lambda_{cr} = \frac{3^{1/3}\alpha(\beta-1)h_0}{4\gamma^{1/3}} + \mathcal{O}(\gamma^{-4/3}), \quad (5.12)$$

$$\delta_2 = \overset{\circ}{k}_{cr} - k_{cr} = -\frac{\alpha(\beta-1)}{\pi} + \mathcal{O}(\gamma^{-1/3}). \quad (5.13)$$

The sign of δ_1 implies whether a bilayer with graded substrate is more stable or more unstable than the corresponding homogeneous substrate. Thus, we summarize the results of the signs of δ_1 and δ_2 as follows

$$\delta_1 \quad \text{or} \quad -\delta_2 \quad \begin{cases} > 0, & \text{if } \alpha < 0, \beta < 1 \quad \text{or} \quad \alpha > 0, \beta > 1, \\ < 0, & \text{if } \alpha > 0, \beta < 1. \end{cases} \quad (5.14)$$

Note that the prerequisite that (5.12) and (5.13) hold is $\beta \sim \mathcal{O}(1)$. Therefore we may allow $\beta > 1$ but a large β is not granted. It can be seen that either $\alpha < 0$, $\beta < 1$ or $\alpha > 0$, $\beta > 1$ indicates a positive δ_1 but a negative δ_2 , suggesting that an increasing modulus distribution will delay surface wrinkling and lead to a larger wavenumber compared to its homogeneous counterpart. Contrariwise, the case $\alpha > 0$, $\beta < 1$, with an exponentially decayed modulus, always gives rise to a more unstable structure and a lower wavenumber. These conclusions further confirm previous results (Cao et al., 2012).

We now check the validity of our asymptotic solutions given by (5.7) and (5.8). Fig. 5 shows how λ_{cr} and k_{cr} depend on γ . We see that the error between asymptotic and exact results is negligible for large γ . Further, we observe from Fig. 5(a) that the asymptotic solution remains valid even for small γ and at $\gamma \approx 2$ the largest error is less than 0.6%. We also see in Fig. 5(b) that (5.8) loses its validity as $\gamma \lesssim 5$. These solutions also demonstrate that a larger mismatch of the stiffness between the film and substrate always tends to destabilize the structure with a higher λ_{cr} but a lower k_{cr} which is consistent with previous results.

Next we investigate the effect of h_0 in Fig. 6. Again the agreement between exact and asymptotic solutions is excellent, and we observe that unless the substrate is homogeneous (Liu and Dai, 2014), the critical stretch is affected by h_0 . Indeed, λ_{cr} in (5.7) depends on h_0 via second and higher order terms for a graded substrate but with factors α and $\beta - 1$ that vanish identically for homogeneous substrates. The effect of h_0 is weak as seen in Fig. 6(a). This results seems unexpected at first sight as the bilayer is more unstable with a thicker film. However, since k_{cr} is proportional to $1/h_0$, a thicker film develops less wrinkles (see Fig. 6(b)). We emphasize that the order relation $\gamma \sim \mathcal{O}(h_0^{-\frac{3}{2}})$ implies that the film is much stiffer than the substrate for extremely thin films.

5.1.2. Moderately stiff film on soft graded substrate: $\gamma \sim \mathcal{O}(h_0^{-1})$

From the leading-order balance analysis of (5.1) we discover an implied relation between γ and kh_0 , i.e. $kh_0 \sim \mathcal{O}(\gamma^{-\frac{1}{3}})$. We now assume that the film is not as stiff and have, instead, $\gamma = \mathcal{O}(h_0^{-1})$. In this case, we have $k = \mathcal{O}(\gamma^{\frac{2}{3}})$ and with $h_0 = a_0\gamma^{-1}$. The

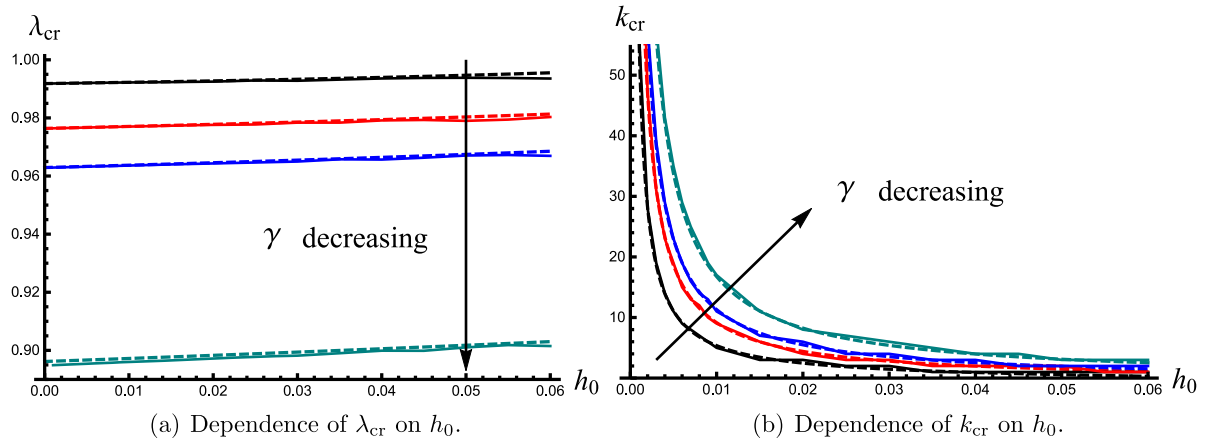


Fig. 6. Comparisons between the asymptotic (dashed line) and exact (solid line) solutions of λ_{cr} and k_{cr} for $\alpha = 1$, $\beta = 0.01$ and $\gamma = 500, 100, 50, 10$ when $\gamma \sim \mathcal{O}(h_0^{-\frac{1}{2}})$.

asymptotic solutions for λ_{cr} and k_{cr} are now

$$\begin{aligned}\lambda_{cr} &= 1 - \varepsilon = 1 - m_0\gamma^{-\frac{2}{3}} - m_1\gamma^{-1} - m_2\gamma^{-\frac{4}{3}} - m_3\gamma^{-\frac{5}{3}} + \dots, \\ k_{cr} &= l_0\gamma^{\frac{2}{3}} + l_1\gamma^{\frac{1}{3}} + l_2 + l_3\gamma^{-\frac{1}{3}} + \dots,\end{aligned}\quad (5.15)$$

where m_i and l_i ($i = 0, 1, 2, \dots$) are constants depending on h_0 , α and β and can be solved from Eqs. (4.16) and (5.4).

Following the same procedure as in the previous case, we obtain the asymptotic solutions:

$$\lambda_{cr} = 1 - \frac{3^{2/3}}{4\gamma^{2/3}} + \frac{3^{1/3}}{160\gamma^{4/3}} (33 - 40\alpha(\beta - 1)\gamma h_0) - \frac{3^{2/3}}{24\gamma^{5/3}} (3 - 2\alpha(\beta - 1)\gamma h_0) + \mathcal{O}(\gamma^{-2}), \quad (5.16)$$

$$k_{cr} = \frac{3^{1/3}}{\pi\gamma^{1/3}h_0} + \frac{\alpha(\beta - 1)}{\pi} - \frac{27}{20\pi\gamma h_0} - \frac{\alpha(\beta - 1)}{2 \cdot 3^{2/3}\pi\gamma^{1/3}} + \mathcal{O}(\gamma^{-2/3}). \quad (5.17)$$

These solutions reduce to (5.9) and (5.10), when either $\alpha = 0$ or $\beta = 1$. Further, the leading order term of (5.16) and the first two terms of (5.17) are identical to those in (5.7) and (5.8). Nevertheless, an interesting difference is that the lowest order where the information of modulus gradient occurs is $\mathcal{O}(\gamma^{-\frac{4}{3}})$ in (5.16) while the corresponding order is $\mathcal{O}(\gamma^{-1})$ in (5.7). Hence, the influence of modulus gradient on the critical stretch λ_{cr} becomes negligible as the modulus mismatch between the film and substrate drops. For the critical wavenumber, the first two terms of (5.17) are consistent with those of (5.8), indicating that the buckled morphology is nearly impervious as order between γ and h_0 varies from $\gamma \sim \mathcal{O}(h_0^{-\frac{3}{2}})$ to $\gamma \sim \mathcal{O}(h_0^{-1})$.

5.1.3. Slightly stiffer film on soft graded substrate: $\gamma \sim \mathcal{O}(h_0^{-\frac{1}{2}})$

Finally, we consider the case $\gamma \sim \mathcal{O}(h_0^{-\frac{1}{2}})$ which implies $k \sim \mathcal{O}(\gamma^{\frac{5}{3}})$, and we obtain

$$\lambda_{cr} = 1 - \frac{3^{2/3}}{4\gamma^{2/3}} + \frac{33 \cdot 3^{1/3}}{160\gamma^{4/3}} - \frac{3^{2/3}}{8\gamma^{5/3}} + \mathcal{O}(\gamma^{-2}), \quad (5.18)$$

$$k_{cr} = \frac{3^{1/3}}{\pi\gamma^{1/3}h_0} - \frac{27}{20\pi\gamma h_0} + \mathcal{O}(\gamma^{1/3}). \quad (5.19)$$

These results are independent of the modulus gradient parameters α , β and the thickness h_0 . Specifically, Eqs. (5.18) and (5.19) coincide exactly with (5.9) and (5.10), respectively, up to the truncated order. This implies that for a slightly stiff film, the graded substrate makes little difference compared to its homogeneous counterpart.

Combining the results for $\gamma \sim \mathcal{O}(h_0^{-\frac{3}{2}})$ and $\gamma \sim \mathcal{O}(h_0^{-1})$, we conclude that for a film/substrate bilayer, where the film thickness is fixed and the shear modulus of the substrate either decays exponentially from the surface or is comparable to the modulus at infinity, the influence of the modulus gradient tends to shift to higher orders as the modulus ratio γ decreases, playing a more and more marginal role in regulating surface wrinkling as well as in shaping the final surface pattern.

5.2. Restricted growth

For a stiff layer coated to a soft substrate, it is known that the critical growth factor g_{cr} leading to wrinkling is close to unity (Alawiye et al., 2019). Therefore, $\varepsilon = g_{cr} - 1$ is small. Following the fundamental assumption in Section 5.1, we assume that α is of $\mathcal{O}(1)$ and $\varepsilon, 1/k, 1/\gamma, h_0$ are small.

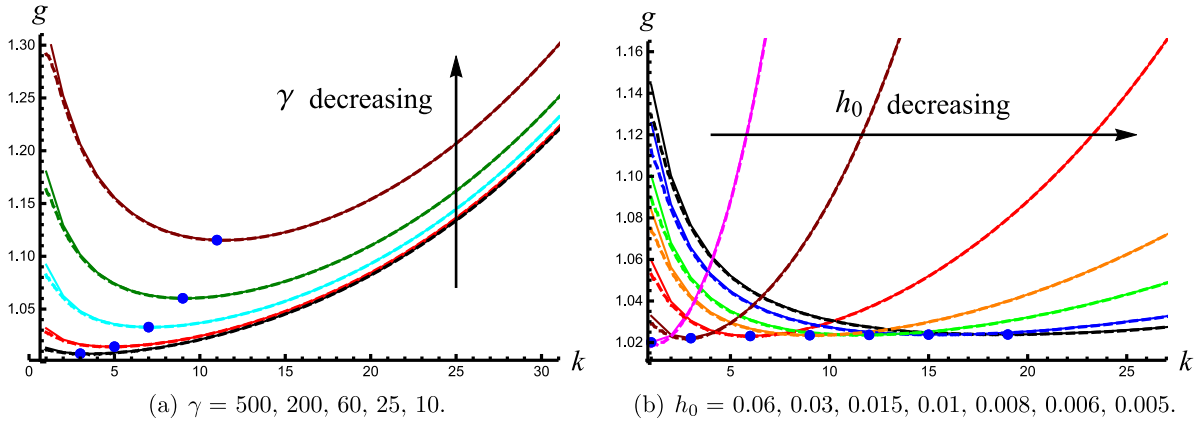


Fig. 7. Comparisons of the bifurcation curves between the approximate (dashed line) and exact (solid line) bifurcation conditions when $\alpha = 1$ and $\beta = 0.01$. The left subfigure displays the dependence of g on k by specifying $h_0 = 0.015$ while the right one exhibits the counterpart for fixed $\gamma = 100$. The blue dots correspond to the critical growth factor g_{cr} associated with the critical wavenumber k_{cr} .

To evaluate the accuracy of the approximate bifurcation condition, we compare in Fig. 7 the bifurcation curves based on the approximate (dashed line) and exact (solid line) bifurcation conditions. The dashed curves are an excellent fit for the solids curves, which indicates the validity of the explicit bifurcation as our new starting point to pursue an asymptotic solution. In Fig. 7 we see that the bifurcation curves have a U-shape. The critical growth factor g_{cr} and the critical wavenumber k_{cr} correspond to the vertical and horizontal coordinates of the local minimum for each curve.

5.2.1. Very stiff film on soft graded substrate: $\gamma \sim \mathcal{O}(h_0^{-\frac{3}{2}})$

We first expand the bifurcation condition $\tilde{\Xi} = 0$ in ε and h_0 . Referring to the order analysis in Section 5.1.1 and by using the leading-order balance and principle of least degeneracy (Liu and Dai, 2014), we arrive at the same order relations as before, namely, $\varepsilon \sim \mathcal{O}(\gamma^{-\frac{2}{3}})$, $h_0 \sim \mathcal{O}(\gamma^{-\frac{2}{3}})$ and $k \sim \mathcal{O}(\gamma^{\frac{1}{3}})$. Therefore, we look for an asymptotic solution of the form

$$\begin{aligned} g_{cr} &= 1 + \varepsilon = 1 + m_0 \gamma^{-\frac{2}{3}} + m_1 \gamma^{-1} + m_2 \gamma^{-\frac{4}{3}} + m_3 \gamma^{-\frac{5}{3}} + \dots, \\ k_{cr} &= l_0 \gamma^{\frac{1}{3}} + l_1 + l_2 \gamma^{-\frac{1}{3}} + l_3 \gamma^{-\frac{2}{3}} + \dots, \end{aligned} \quad (5.20)$$

where m_i and l_i ($i = 0, 1, 2, \dots$) are constants to be determined.

Following the same procedure given in Section 5.1.1, we derive the following formulas

$$\begin{aligned} g_{cr} &= 1 + \frac{3^{2/3}}{4\gamma^{2/3}} + \frac{3^{1/3}\alpha(\beta-1)h_0}{4\gamma^{1/3}} - \frac{1}{480} \left(\frac{9 \cdot 3^{1/3}}{\gamma^{4/3}} + \frac{40 \cdot 3^{2/3}\alpha(\beta-1)h_0}{\gamma^{2/3}} + 100\alpha^2(\beta-1)^2 h_0^2 \right) \\ &\quad + \frac{1}{720} \left(\frac{90 \cdot 3^{2/3}}{\gamma^{5/3}} + \frac{81\alpha(\beta-1)h_0}{\gamma} + \frac{30 \cdot 3^{1/3}\alpha^2(\beta^2-3\beta+2)h_0^2}{\gamma^{1/3}} \right. \\ &\quad \left. + 10 \cdot 3^{2/3}\alpha^3(10\beta^3-32\beta^2+33\beta-11)\gamma^{1/3}h_0^3 \right) + \mathcal{O}(\gamma^{-2}), \end{aligned} \quad (5.21)$$

$$\begin{aligned} k_{cr} &= \frac{3^{1/3}}{\pi\gamma^{1/3}h_0} + \frac{\alpha(\beta-1)}{\pi} - \frac{1}{60\pi} \left(\frac{81}{\gamma h_0} + \frac{10 \cdot 3^{1/3}\alpha(\beta-1)}{\gamma^{1/3}} + 35 \cdot 3^{2/3}\alpha^2(\beta-1)^2 \gamma^{1/3} h_0 \right) \\ &\quad - \frac{\alpha(\beta-1)}{180\pi} \left(\frac{42 \cdot 3^{2/3}}{\gamma^{2/3}} - 30\alpha(2\beta-3)h_0 - 5 \cdot 3^{1/3}\alpha^2(61\beta^2-130\beta+65)\gamma^{2/3} h_0^2 \right) \\ &\quad + \mathcal{O}(\gamma^{-1}). \end{aligned} \quad (5.22)$$

For a homogeneous substrate, Eqs. (5.21) and (5.22) simplify to

$$g_{cr} = 1 + \frac{3^{2/3}}{4\gamma^{2/3}} - \frac{3 \cdot 3^{1/3}}{160\gamma^{4/3}} + \frac{3^{2/3}}{8\gamma^{5/3}} + \mathcal{O}(\gamma^{-2}), \quad (5.23)$$

$$k_{cr} = \frac{3^{1/3}}{\pi\gamma^{1/3}h_0} - \frac{27}{20\pi\gamma h_0} + \mathcal{O}(\gamma^{-1}) \quad \text{or} \quad (nh_0)_{cr} = \frac{3^{1/3}}{\gamma^{1/3}} - \frac{27}{20\gamma} + \mathcal{O}(\gamma^{-5/3}). \quad (5.24)$$

We emphasize that the leading order terms of (5.23) and (5.24)₂ are the same as those in Alawiye et al. (2019), where there is no growth in the substrate and only film growth is considered. This reinforces our conclusion in Liu et al. (2021) that growth gradient has a little effect on the critical buckling load and the associated buckling pattern. Further, it can be seen that the thickness h_0 and the parameters related to modulus gradient α , β are included at higher order terms. So the dominant factor that affects the critical buckling state is still γ . The same conclusion has already been observed in the compression case.

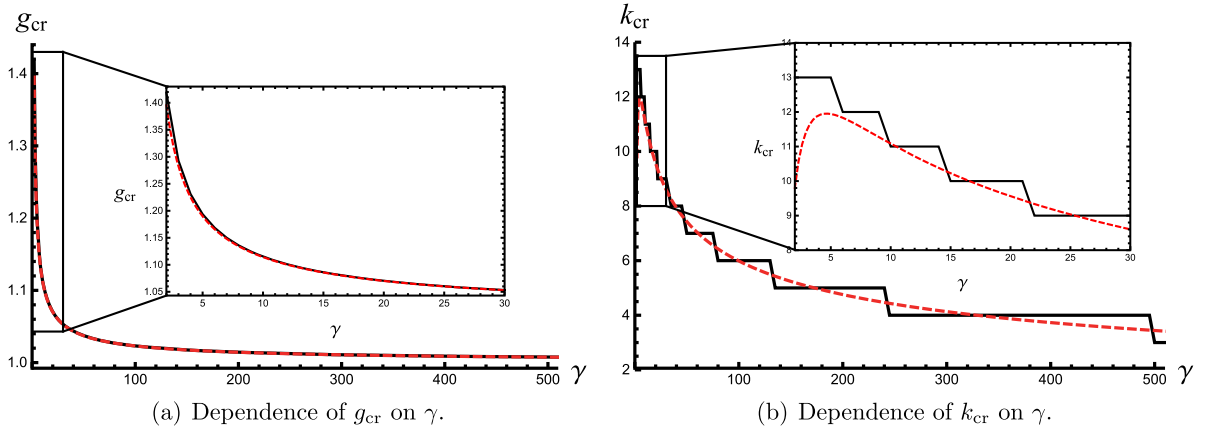


Fig. 8. Comparisons between the asymptotic (dashed line) and exact (solid line) solutions of g_{cr} and k_{cr} for $\alpha = 1$, $\beta = 0.01$, and $h_0 = 0.015$ when $\gamma \sim \mathcal{O}(h_0^{-\frac{2}{3}})$.

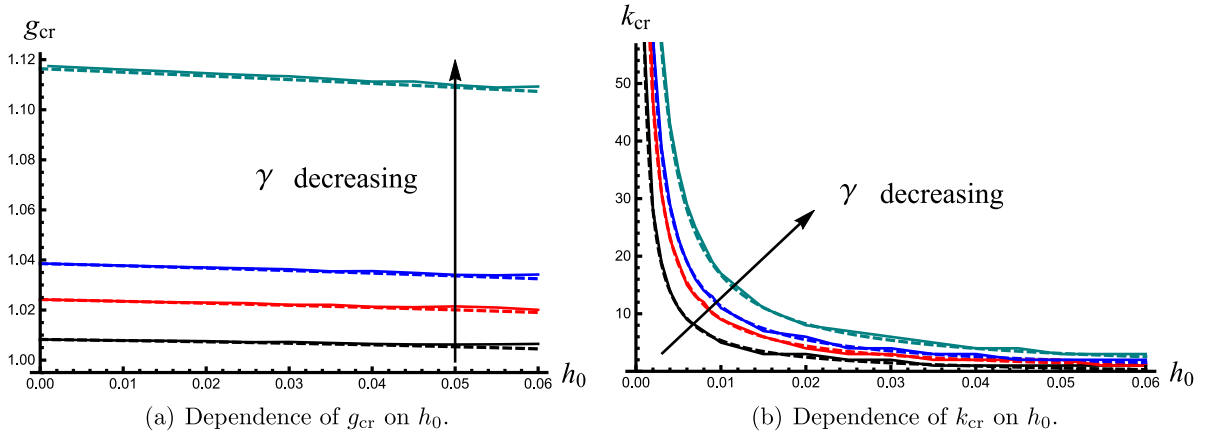


Fig. 9. Comparisons between the asymptotic (dashed line) and exact (solid line) solutions of g_{cr} and k_{cr} for $\alpha = 1$, $\beta = 0.01$ and $\gamma = 500, 100, 50, 10$ when $\gamma \sim \mathcal{O}(h_0^{-\frac{2}{3}})$.

Fig. 8 illustrates the critical growth factor g_{cr} and the critical wavenumber k_{cr} as functions of the modulus ratio γ when $\alpha = 1$, $\beta = 0.01$, and $h_0 = 0.015$. The dashed lines correspond to the asymptotic solution while the solid lines represent the exact solution. We note the surprisingly good agreement between the exact and asymptotic solutions, even when $\gamma \approx 5$. It implies that the general order relation $\varepsilon \sim \mathcal{O}(\gamma^{-\frac{2}{3}})$ captures well surface instability in hyperelastic bilayers.

We plot the relations of g_{cr} , k_{cr} and h_0 in Fig. 9 to further validate our asymptotic solutions. We found from the second order term in (5.21) that the film thickness h_0 starts to affect the critical growth factor g_{cr} , as confirmed in Fig. 9(a). Note that h_0 does not impact the onset of surface wrinkling for a homogeneous substrate through (5.23), but it will change the wavenumber, as shown in (5.24). We conclude that the asymptotic solutions are excellent approximations to describe the onset of surface instability and the corresponding pattern.

5.2.2. Moderately stiff film on soft graded substrate: $\gamma \sim \mathcal{O}(h_0^{-1})$

When $\gamma \sim \mathcal{O}(h_0^{-1})$, $k \sim \mathcal{O}(\gamma^{\frac{2}{3}})$ we obtain the following asymptotic solutions

$$g_{cr} = 1 + \frac{3^{2/3}}{4\gamma^{2/3}} - \frac{3^{1/3}}{160\gamma^{4/3}} (3 - 40\alpha(\beta - 1)\gamma h_0) + \frac{3^{2/3}}{24\gamma^{5/3}} (3 - 2\alpha(\beta - 1)\gamma h_0) + \mathcal{O}(\gamma^{-2}), \quad (5.25)$$

$$k_{cr} = \frac{3^{1/3}}{\pi\gamma^{1/3}h_0} + \frac{\alpha(\beta - 1)}{\pi} - \frac{27}{20\pi\gamma h_0} - \frac{\alpha(\beta - 1)}{2 \cdot 3^{2/3}\pi\gamma^{1/3}} + \mathcal{O}(\gamma^{-2/3}). \quad (5.26)$$

We note that α and β first appear at $\mathcal{O}(\gamma^{-\frac{4}{3}})$, which is higher than the counterpart in (5.21). Hence, the effect of a modulus gradient becomes weaker as the modulus ratio γ declines.

Table 1

Comparisons between the exact and asymptotic solutions of g_{cr} as γ is not large. All other parameters are specified by $h_0 = 0.015$, $\alpha = 1$ and $\beta = 0.01$. We denote Δ the relative error between the exact and asymptotic solutions.

γ	Exact g_{cr}	$\gamma = \mathcal{O}(h_0^{-\frac{1}{2}})$	Δ	$\gamma = \mathcal{O}(h^{-1})$	Δ	$\gamma = \mathcal{O}(h_0^{-\frac{1}{2}})$	Δ
9	1.12453	1.12322	0.11682%	1.12344	0.09717%	1.12542	-0.07883%
8	1.1357	1.13416	0.13520%	1.13441	0.11375%	1.13644	-0.06531%
7	1.14986	1.14787	0.17289%	1.14814	0.14918%	1.15024	-0.03307%
6	1.16846	1.16566	0.23979%	1.16597	0.21312%	1.16813	0.02766%
5	1.19371	1.18985	0.32358%	1.19022	0.2929%	1.19247	0.10434%
4	1.23101	1.22511	0.47965%	1.22556	0.44322%	1.22791	0.2522%
3	1.29281	1.28236	0.80875%	1.28294	0.76343%	1.28542	0.57199%
2	1.41873	1.39527	1.65369%	1.39613	1.59297%	1.39876	1.40772%

5.2.3. Slightly stiff film on soft graded substrate: $\gamma \sim \mathcal{O}(h_0^{-\frac{1}{2}})$

The last case, $\gamma \sim \mathcal{O}(h_0^{-\frac{1}{2}})$ and $k \sim \mathcal{O}(\gamma^{\frac{5}{3}})$, corresponds to a slightly stiff film coated to a soft graded substrate, for which, we have

$$g_{cr} = 1 + \frac{3^{2/3}}{4\gamma^{2/3}} - \frac{3^{4/3}}{160\gamma^{4/3}} + \frac{3^{2/3}}{8\gamma^{5/3}} + \mathcal{O}(\gamma^{-2}), \quad (5.27)$$

$$k_{cr} = \frac{3^{1/3}}{\pi\gamma^{1/3}h_0} - \frac{27}{20\pi\gamma h_0} + \mathcal{O}(\gamma^{1/3}), \quad (5.28)$$

which does not depend on α and β . Meanwhile, Eqs. (5.27) and (5.28) are identical to (5.23) and (5.24)₁ up to the retained order, respectively, implying that a homogeneous substrate can indeed replace a graded one when estimating the critical buckling threshold and the associated buckling pattern. In addition, we give the performance of the asymptotic solutions (5.21), (5.25) and (5.27) when γ is slightly greater than unity in Table 1. Again, the relative errors are small even when $\gamma \approx 2$. The solution of $\gamma = \mathcal{O}(h_0^{-\frac{1}{2}})$ yields the best prediction.

We conclude that in the confined growth scenario when both α and β are of $\mathcal{O}(1)$ (or small β) and both h_0 and $1/\gamma$ are small, the influence of the modulus gradient on pattern formation in a stiff film bonded to a compliant graded substrate is negligible. For smaller γ , the modulus gradient becomes irrelevant.

6. Asymptotic solution when β is large

When the modulus ratio β is large we use the WKB approximation (4.9). Following the method given in Section 4.1, we obtain

$$S_1 = -\frac{\alpha(1-\beta)\lambda \exp(-\alpha(\lambda y - h_0))}{2(\beta + (1-\beta)\exp(-\alpha(\lambda y - h_0)))}, \quad (6.1)$$

$$S_1' = -\frac{\alpha^2(\beta-1)\beta\lambda^2 \exp(-\alpha(\lambda y - h_0))}{2(\beta(\exp(-\alpha(\lambda y - h_0)) - 1) + 1)^2}. \quad (6.2)$$

Both S_1 and S_1' are negative under the assumption $\beta \gg 1$ and $\alpha > 0$ which implies that S_1 attains its local maximum at $y = h_0/\lambda$ with extreme value given by

$$S_{1\max} = \frac{1}{2}\alpha(\beta-1)\lambda. \quad (6.3)$$

It can be estimated from (6.1) and (6.3) that a boundary layer exists after which S_1 decreases. However, near the surface $y = h_0/\lambda$, it is of $\mathcal{O}(\beta)$. The first term in (4.9) (kS_0) is of $\mathcal{O}(\gamma^{\frac{1}{3}})$ and the second term (S_1) is of $\mathcal{O}(\beta)$. Bearing in mind that a valid asymptotic expansion requires that the latter terms are strictly smaller than the previous one, we consider a limit case $\beta = \mathcal{O}(\gamma^{\frac{1}{3}})$, which means that the first and second terms are of the same order $\mathcal{O}(\gamma^{\frac{1}{3}})$ in the boundary layer, and the first term is much larger outside the boundary layer. Hence, we write

$$\beta = b_0\gamma^{\frac{1}{3}}, \quad (6.4)$$

where b_0 is a constant of $\mathcal{O}(1)$. We seek an asymptotic solution for λ_{cr} and k_{cr} the same as (5.6). By applying the regular solution procedure, it is found that the coefficients l_0 and m_0 satisfy the following algebraic equations

$$2\pi^6 a_0^3 l_0^6 - 24\pi^4 a_0 m_0 l_0^4 + 12\pi^3 l_0^3 + 18\pi^2 \alpha b_0 l_0^2 + 3\pi \alpha^2 b_0^2 l_0 - 3\alpha^3 b_0^3 = 0, \quad (6.5)$$

$$16\pi^6 a_0^3 l_0^6 - 144\pi^4 a_0 m_0 l_0^4 + 60\pi^3 l_0^3 + 72\pi^2 \alpha b_0 l_0^2 + 9\pi \alpha^2 b_0^2 l_0 - 6\alpha^3 b_0^3 = 0, \quad (6.6)$$

where a_0 has been defined in (5.5).

Unfortunately, Eqs. (6.5) and (6.6) give rise to a polynomial equation of degree six in l_0 , which has no general solution. To overcome this difficulty, we resort to curve fitting using a specific function and the regression analysis yields

$$l_0 = 0.170341 \ln \left(\frac{\alpha\beta}{\gamma^{1/3}} + 0.552186 \right) + \frac{0.564331}{(h_0\gamma^{2/3})^{0.90481}} - 0.00854314, \quad (6.7)$$

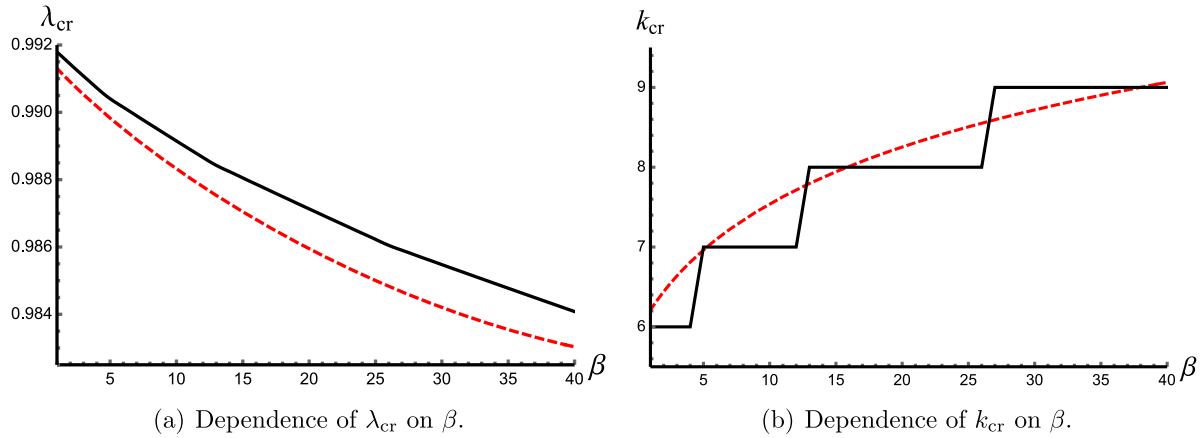


Fig. 10. Comparisons between the asymptotic (dashed line) and exact (solid line) solutions of λ_{cr} and k_{cr} for $\gamma = 500$, $h_0 = 0.01$, $\alpha = 1$ when $\beta = \mathcal{O}(\gamma^{1/3})$.

$$m_0 = -\frac{\alpha^3 \beta^3}{8\pi^4 \gamma^{5/3} h_0 l_0^4} + \frac{\alpha^2 \beta^2}{8\pi^3 \gamma^{4/3} h_0 l_0^3} + \frac{3\alpha\beta}{4\pi^2 \gamma h_0 l_0^2} + \frac{1}{2\pi \gamma^{2/3} h_0 l_0} + \frac{1}{12} \pi^2 \gamma^{4/3} h_0^2 l_0^2. \quad (6.8)$$

We see that the critical wavenumber is affected by the modulus ratio γ only through a logarithm term. A similar dependence was also observed in growing layers (Ciarletta and Fu, 2015; Jin et al., 2018).

The leading-order solutions of the critical bifurcation thresholds read $\lambda_{cr} = 1 - m_0/\gamma^{2/3}$ and $g_{cr} = 1 + m_0/\gamma^{2/3}$ while the critical wavenumber is $k_{cr} = l_0 \gamma^{-1/3}$. We then illustrate the critical stretch and the critical wavenumber as functions of β in Fig. 10 when $\gamma = 500$, $h_0 = 0.01$, $\alpha = 1$. For comparison, both the leading-order asymptotic solution (dashed line) and the exact one (solid line) are plotted. It is emphasized that an obvious gap occurs as the vertical axial ranges from 0.983 to 0.992. In fact, the maximum error for the critical strain $1 - \lambda_{cr}$ is around 5% in Fig. 10(a). On the other hand, we find that the leading-order coefficients are only valid when β is less than 40, which is the termination of β in Fig. 10. Furthermore, the critical stretch λ_{cr} is a decreasing function of β , indicating that a greater β tends to delay the instability. From Fig. 10(b) we see that the critical wavenumber is an increasing function of β . So a larger β will produce more wrinkles, which is consistent with the results in Cao et al. (2012).

7. Discussions and conclusions

We investigated the surface wrinkling of a stiff film resting on a soft graded substrate engendered by in-plane compression or restricted growth. A theoretical model was used to identify the onset of surface wrinkling within the framework of nonlinear elasticity and by use of the incremental theory without specifying a material model and a modulus function of substrate. An exact bifurcation condition was presented by means of the Stroh formulation and the impedance matrix method (Liu et al., 2022; Wang et al., 2023). In the short wavelength limit, the WKB technique was applied to deal with the eigenvalue problem of ODEs with variable coefficients, and as a result an explicit bifurcation condition was obtained. By considering an exponential modulus function, the effectiveness of the approximate bifurcation condition was validated based on the exact one, and the valid domains where the WKB expansion is effective were identified for various parameters. For other functional forms of the modulus gradient, say a linear function or a power function for instance, the WKB analysis as well as the solution procedure presented in this paper are both applicable provided that the expansions (4.9) and (4.21) are valid. Also, this condition may lead to restrictions on allowable parameters appearing in the modulus gradient function to ensure the validity of the asymptotic analysis.

We determined the order relations and showed that the modulus ratio γ is extremely significant in regulating the onset of surface wrinkling in bilayer systems as found before (Liu et al., 2021, 2022) and that the critical relation $\varepsilon \sim \mathcal{O}(\gamma^{-2/3})$ is consistent with most existing studies on pattern formation in film/substrate structures (Cai and Fu, 1999; Liu and Dai, 2014; Cai and Fu, 2019; Jin et al., 2018; Jia et al., 2018; Wang et al., 2023). However, if surface wrinkling is replaced by a Euler-type buckling with mode number 1 or 2, the aspect ratio of the whole structure becomes dominant (Liu, 2023).

When β is not large, we found that the asymptotic solutions for the critical loads and the critical wavenumber give an excellent approximation and that these solutions do not strongly depend on the modulus gradient as it only appears in higher-order terms. However, as γ decreases, and unlike a homogeneous bilayer, the film thickness h_0 starts to alter the critical load and unexpectedly a thicker film tends to destabilize the structure. Furthermore, surface wrinkling is more likely if the shear modulus of the substrate decays away from the surface.

To compare the axial compression case to the confined growth case, we define the critical thickness h_{cr} at the bifurcation point:

$$h_{cr} = h_0 + \frac{3^{2/3} h_0}{4\gamma^{2/3}} + \frac{3^{1/3} \alpha(\beta - 1) h_0^2}{4\gamma^{1/3}} + \mathcal{O}(\gamma^{-4/3}), \quad \text{uniaxial compression,} \quad (7.1)$$

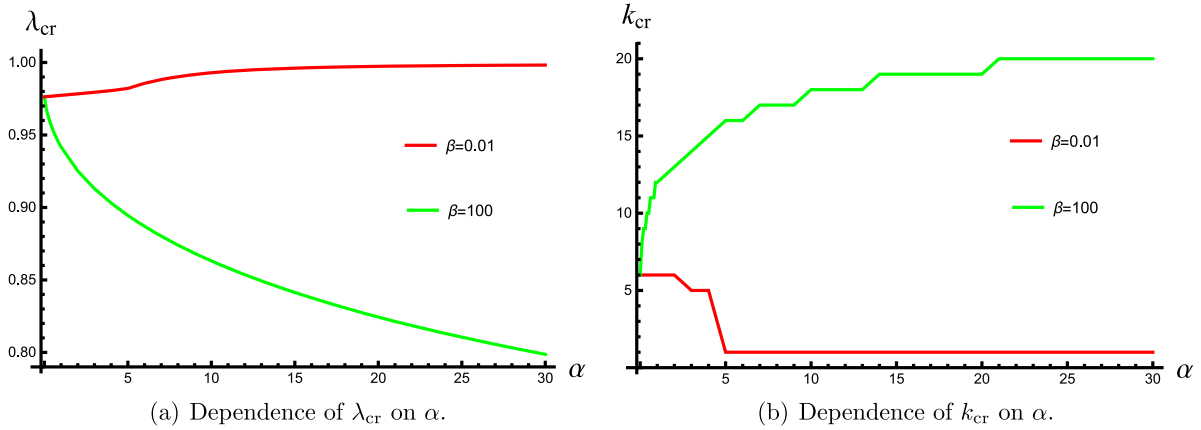


Fig. 11. Influence of the grading parameter α on the critical stretch and the critical wavenumber with $\gamma = 100$ and $h_0 = 0.015$. We are concerned with the behavior as $\alpha \geq 0$.

$$h_{cr} = h_0 + \frac{3^{2/3} h_0}{2\gamma^{2/3}} + \frac{3^{1/3} \alpha (\beta - 1) h_0^2}{2\gamma^{1/3}} + \mathcal{O}(\gamma^{-4/3}), \quad \text{growth.} \quad (7.2)$$

The small difference at $\mathcal{O}(\gamma^{-2/3})$ is due to the fact that the structure is allowed to grow in both the horizontal and the vertical directions. If we only consider horizontal growth, the corresponding formulas would be identical up to $\mathcal{O}(\gamma^{-4/3})$.

In the case of large β and assuming $\beta \sim \mathcal{O}(\gamma^{1/3})$, we found the leading-order solution from a regression analysis. In this case, the parameters related to modulus gradient emerge in the leading-order terms, showing that the modulus gradient cannot be neglected when the shear modulus of the substrate increases from its surface.

To study the role of grading parameter α that controls how fast the shear modulus of the half-space decays or grows from its surface, we show in Fig. 11(a) the relation between λ_{cr} and α and in Fig. 11(b) the relation between k_{cr} and α . We consider two scenarios, namely, exponentially decaying modulus ($\beta = 0.01$) and the reverse one ($\beta = 100$). When $\beta = 0.01$, we observe from Fig. 11 that λ_{cr} gradually ascends but k_{cr} experiences a sudden drop from 5 to 1 as $\alpha \approx 5$, and the λ_{cr} curve is non-smooth as well. With increasing α , the shear modulus of substrate will decay faster and the system will behave like triple layer structure. If a compliant substrate is coated with two stiff layers a mode transition has been observed as the intermediate layer becomes softening (Zhou et al., 2022). This may explain the jump behavior at $\alpha \approx 5$. Indeed, a greater α is equivalent to reducing either the thickness or the modulus of the middle layer. In doing so, the tendency of k_{cr} - α curve in Fig. 11(b) (for $\beta = 0.01$) is consistent with the conclusion in Cheng et al. (2014). Moreover, the grading parameter only generates a minor correction to λ_{cr} but creates a large change in the critical mode. When $\alpha > 5$, the critical wavenumber remains one which indicates that α does not affect the pattern.

When $\beta = 100$, with an exponentially growing modulus in the substrate, the results are different. Then both λ_{cr} and k_{cr} are highly dependent on α . In particular, the critical stretch λ_{cr} is a monotonically decreasing function of α while the critical wavenumber k_{cr} is a monotonically increasing function of α . As α goes to infinity λ_{cr} will approach a limit value similar to the one obtained for instability of a soft wire embedded into a half-space. Indeed, for $\alpha = 5000$, we find $\lambda_{cr} = 0.5724$, similar to the Biot value 0.543 at which surface instability in a compressed half-space takes place (Biot, 1963).

Finally, we summarize the effect of the modulus gradient. If the grading parameter $\alpha \sim \mathcal{O}(1)$, our analytical solutions show a relatively small role of the grading for an exponentially decayed modulus in the substrate as the modulus gradient only affects high-order terms. If, however, the modulus increases away from the interface, then the gradient plays a leading role through a first-order logarithm dependence. For α large, corresponding to a change of modulus in a very thin region, the grading effect has little influence on the critical state but has a very pronounced effect in shaping the pattern for an exponentially decaying modulus. Conversely, for a growing modulus, the modulus gradient has a strong effect on both the critical stretch and the associated pattern. As $\alpha \rightarrow \infty$ the bilayer degenerates to a half-space with a soft line inclusion. Then, the classical Biot instability is recovered but with a finite wavenumber. The results presented here give a systematic way to consider wrinkling instabilities in bilayered grading material and a natural complement to computational studies.

CRediT authorship contribution statement

Rui-Cheng Liu: Writing – original draft, Investigation, Formal analysis, Software. **Yang Liu:** Writing – review & editing, Writing – original draft, Methodology, Funding acquisition, Formal analysis, Conceptualization. **Alain Goriely:** Writing – review & editing, Writing – original draft, Methodology, Funding acquisition, Formal analysis, Conceptualization.

Declaration of competing interest

The authors declare that they have no known competing financial interests or personal relationships that could have appeared to influence the work reported in this paper.

Data availability

Data will be made available on request.

Acknowledgments

Y.L. acknowledges the financial support from the National Natural Science Foundation of China (Project Nos. 12072227 and 12021002). Y.L. and A.G. acknowledge the UKRI Horizon Europe Guarantee MSCA (Marie Skłodowska-Curie Actions) Postdoctoral Fellowship (EPSRC Grant No. EP/Y030559/1). The author would like to thank the Isaac Newton Institute for Mathematical Sciences for support and hospitality during the programme Uncertainty Quantification and Stochastic Modelling of Materials when work on this paper was undertaken. This work was supported by EPSRC, UK Grant Number EP/R014604/1. A.G. acknowledges support from the Engineering and Physical Sciences Research Council of Great Britain under Research Grant No. EP/R020205/1. For the purpose of Open Access, the author has applied a CC BY public copyright license to any Author Accepted Manuscript (AAM) version arising from this submission.

References

- Alawiye, H., Farrell, P.E., Goriely, A., 2020. Revisiting the wrinkling of elastic bilayers II: Post-bifurcation analysis. *J. Mech. Phys. Solids* 143, 104053.
- Alawiye, H., Kuhl, E., Goriely, A., 2019. Revisiting the wrinkling of elastic bilayers I: linear analysis. *Phil. Trans. R. Soc. A* 377, 20180076.
- Autumn, K., Sitti, M., Liang, Y.A., Peattie, A.M., Hansen, W.R., Sponberg, S., Kenny, T.W., Fearing, R., Israelachvili, J.N., Full, R.J., 2002. Evidence for van der Waals adhesion in gecko setae. *Proc. Natl. Acad. Sci. USA* 99 (19), 12252–12256.
- Balbi, V., Destrade, M., Goriely, A., 2020. Mechanics of human brain organoids. *Phys. Rev. E* 101 (2), 022403.
- Balbi, V., Kuhl, E., Ciarletta, P., 2015. Morphoelastic control of gastro-intestinal organogenesis: Theoretical predictions and numerical insights. *J. Mech. Phys. Solids* 78, 493–510.
- Ben Amar, M., Goriely, A., 2005. Growth and instability in elastic tissues. *J. Mech. Phys. Solids* 53, 2284–2319.
- Bigoni, D., Ortiz, M., Needleman, A., 1997. Effect of interfacial compliance on bifurcation of a layer bonded to a substrate. *Int. J. Solids Struct.* 34, 4305–4326.
- Biot, M.A., 1963. Surface instability of rubber in compression. *Appl. Sci. Res.* 12, 168–182.
- Biryukov, S.V., Gulyaev, Y.V., Krylov, V.V., Plessky, V.P., 1995. *Surface Acoustic Waves in Inhomogeneous Media*. Springer Berlin, Heidelberg.
- Biryukov, S.V., 1985. Impedance method in the theory of elastic surface waves. *Sov. Phys. Acoust.* 31, 350–354.
- Budday, S., Kuhl, E., Hutchinson, J.W., 2015. Period-doubling and period-tripling in growing bilayered systems. *Philos. Mag.* 95, 3208–3224.
- Budday, S., Steinmann, P., Kuhl, E., 2014. The role of mechanics during brain development. *J. Mech. Phys. Solids* 72, 75–92.
- Cai, Z.X., Fu, Y.B., 1999. On the imperfection sensitivity of a coated elastic half-space. *Proc. R. Soc. Lond. Ser. A Math. Phys. Eng. Sci.* 455, 3285–3309.
- Cai, Z.X., Fu, Y.B., 2000. Exact and asymptotic stability analyses of a coated elastic half-space. *Int. J. Solids Struct.* 37, 3101–3119.
- Cai, Z.X., Fu, Y.B., 2019. Effects of pre-stretch, compressibility and material constitution on the period-doubling secondary bifurcation of a film/substrate bilayer. *Int. J. Non-Linear Mech.* 115, 11–19.
- Cao, Y.P., Jia, F., Zhao, Y., Feng, X.Q., Yu, S.W., 2012. Buckling and post-buckling of a stiff film resting on an elastic graded substrate. *Int. J. Solids Struct.* 49, 1656–1664.
- Cao, Y.P., Zheng, X.P., Li, B., Feng, X.Q., 2009. Determination of the elastic modulus of micro- and nanowires/tubes using a buckling-based metrology. *Scr. Mater.* 61, 1044–1047.
- Chan, E.P., Page, K.A., Im, S.H., Patton, D.L., Huang, R., Stafford, C.M., 2009. Viscoelastic properties of confined polymer films measured via thermal wrinkling. *Soft Matter* 5, 4638–4641.
- Chan, E.P., Smith, E.J., Hayward, R.C., Crosby, A.J., 2008. Surface wrinkles for smart adhesion. *Adv. Mater.* 20 (4), 711–716.
- Chen, Z., Chen, W.Q., Song, J.Z., 2017. Buckling of a stiff thin film on an elastic graded compliant substrate. *Proc. R. Soc. Lond. Ser. A Math. Phys. Eng. Sci.* 473, 20170410.
- Chen, Z., Zhang, X.F., Song, J.Z., 2018. Surface wrinkling of an elastic graded layer. *Soft Matter* 14, 8717–8723.
- Cheng, H.Y., Zhang, Y.H., Huang, K.C., Rogers, J.A., Huang, Y.G., 2014. Buckling of a stiff thin film on a pre-strained bi-layer substrate. *Int. J. Solids Struct.* 51, 3113–3118.
- Ciarletta, P., Fu, Y.B., 2015. A semi-analytical approach to Biot instability in a growing layer: Strain gradient correction, weakly non-linear analysis and imperfection sensitivity. *Int. J. Non-Linear Mech.* 75, 38–45.
- Coman, C.D., Destrade, M., 2008. Asymptotic results for bifurcations in pure bending of rubber blocks. *Q. J. Mech. Appl. Math.* 61 (3), 395–414.
- Dai, H.-H., Liu, Y., 2014. Critical thickness ratio for buckled and wrinkled fruits and vegetables. *Europhys. Lett.* 108 (4), 44003.
- De Pascalis, R., Lisi, F., Napoli, G., 2023. Solid Electrolyte Interphase elastic instability in Li-ion battery anodes. *Extreme Mech. Lett.* 61, 102014.
- Diab, M., Kim, K.S., 2014. Ruga-formation instabilities of a graded stiffness boundary layer in a neo-Hookean solid. *Proc. R. Soc. Lond. Ser. A Math. Phys. Eng. Sci.* 470, 20140218.
- Dorris, J.F., Nemat-Nasser, S., 1980. Instability of a layer on a half space. *J. Appl. Mech.* 47 (2), 304–312.
- van den Ende, D.A., Kamminga, J.D., Boersma, A., Andritsch, T., Steeneken, P.G., 2013. Voltage-controlled surface wrinkling of elastomeric coatings. *Adv. Mater.* 27, 489–512.
- Eskandari, M., Javili, A., Kuhl, E., 2016. Elastosis during airway wall remodeling explains multiple co-existing instability patterns. *J. Theoret. Biol.* 403, 209–218.
- Eskandari, M., Pfaller, M.R., Kuhl, E., 2013. On the role of mechanics in chronic lung disease. *Materials* 6, 5639–5658.
- Fu, Y.B., 1998. Some asymptotic results concerning the buckling of a spherical shell of arbitrary thickness. *Int. J. Non-Linear Mech.* 33 (6), 1111–1122.
- Fu, Y.B., 2005. An integral representation of the surface-impedance tensor for incompressible elastic materials. *J. Elasticity* 81, 75–90.
- Fu, Y.B., Ciarletta, P., 2015. Buckling of a coated elastic half-space when the coating and substrate have similar material properties. *Proc. R. Soc. Lond. Ser. A Math. Phys. Eng. Sci.* 471, 20140979.
- Fu, Y.B., Mielke, A., 2002. A new identity for the surface-impedance matrix and its application to the determination of surface-wave speeds. *Proc. R. Soc. Lond. Ser. A Math. Phys. Eng. Sci.* 458, 2523–2543.
- Goriely, A., 2017. *The Mathematics and Mechanics of Biological Growth*. Springer, New York.
- Haughton, D.M., Chen, Y.C., 2003. Asymptotic bifurcation results for the eversion of elastic shells. *Z. Angew. Math. Phys.* 54, 191–211.
- Hinch, E.J., 1991. *Perturbation Methods*. Cambridge University Press.
- Holland, M., Budday, S., Goriely, A., Kuhl, E., 2018. Symmetry breaking in wrinkling patterns: Gyri are universally thicker than sulci. *Phys. Rev. Lett.* 121, 228002.
- Huang, R., 2005. Kinetic wrinkling of an elastic film on a viscoelastic substrate. *J. Mech. Phys. Solids* 53, 63–89.

- Huang, R., Suo, Z., 2002. Instability of a compressed elastic film on a viscous layer. *Int. J. Solids Struct.* 39, 1791–1802.
- Hutchinson, J.W., 2013. The role of nonlinear substrate elasticity in the wrinkling of thin films. *Phil. Trans. R. Soc. A* 371, 20120422.
- Im, S.H., Huang, R., 2008. Wrinkle patterns of anisotropic crystal films on viscoelastic substrates. *J. Mech. Phys. Solids* 56, 3315–3330.
- Jia, F., Cao, Y.P., Zhao, Y., Feng, X.Q., 2014. Buckling and surface wrinkling of an elastic graded cylinder with elastic modulus arbitrarily varying along radial direction. *Int. J. Appl. Mech.* 6 (1), 1450003.
- Jia, F., Pearce, S., Goriely, A., 2018. Curvature delays growth-induced wrinkling. *Phys. Rev. E* 98, 033003.
- Jin, L.S., Liu, Y., Cai, Z.X., 2018. Asymptotic solutions on the circumferential wrinkling of growing tubular tissues. *Int. J. Eng. Sci.* 128, 31–43.
- Khare, K., Zhou, J.H., Wang, S., 2009. Tunable open-channel microfluidics on soft poly(dimethyl-siloxane)(PDMS) substrates with sinusoidal grooves. *J. Am. Chem. Soc.* 131 (21), 7279–7289.
- Kücken, M., Newell, A.C., 2004. A model for fingerprint formation. *Europhys. Lett.* 68 (1), 141–146.
- Lee, J., Jung, S., Kim, W., 2021. Dependence of the effective surface tension of liquid phase eutectic gallium indium on wrinkles of the surface oxide. *Extreme Mech. Lett.* 48, 101386.
- Lee, S.G., Lee, D.Y., Lim, H.S., Lee, D.H., Lee, S., Cho, K., 2010. Switchable transparency and wetting of elastomeric smart windows. *Adv. Mater.* 22 (44), 5013–5017.
- Lee, D., Triantafyllidis, N., Barber, J.R., Thouless, M.D., 2008. Surface instability of an elastic half space with material properties varying with depth. *J. Mech. Phys. Solids* 56, 858–868.
- Lee, G., Zarei, M., Wei, Q., Zhu, Y., Lee, S.G., 2022. Surface wrinkling for flexible and stretchable sensors. *Small* 18, 2203491.
- Li, B., Cao, Y.P., Feng, X.Q., 2011a. Growth and surface folding of esophageal mucosa: A biomechanical model. *J. Biomech.* 44, 182–188.
- Li, B., Cao, Y.P., Feng, X.Q., Gao, H., 2011b. Surface wrinkling of mucosa induced by volumetric growth: Theory, simulation and experiment. *J. Mech. Phys. Solids* 59, 758–774.
- Li, B., Cao, Y.P., Feng, X.Q., Gao, H., 2012. Mechanics of morphological instabilities and surface wrinkling in soft materials: a review. *Soft Matter* 8 (5728).
- Li, Z.W., Zhai, Y., Wang, Y., Wendland, G.M., Yin, X.B., Xiao, J.L., 2017. Harnessing surface wrinkling-cracking patterns for tunable optical transmittance. *Adv. Opt. Mater.* 5 (19), 1700425.
- Liu, Y., 2018. Axial and circumferential buckling of a hyperelastic tube under restricted compression. *Int. J. Non-Linear Mech.* 98, 145–153.
- Liu, Y., 2023. Higher order solution to the Euler buckling threshold for compressible hyperelastic bilayers. *Acta Mech. Sin.* 39, 422379.
- Liu, Y., Dai, H.-H., 2014. Compression of a hyperelastic layer-substrate structure: Transitions between buckling and surface modes. *Int. J. Eng. Sci.* 80, 74–89.
- Liu, R.C., Jin, L.S., Liu, Y., Cai, Z.X., 2022. An experimental study of morphological formation in bilayered tubular structures driven by swelling/growth. *Math. Mech. Solids* 27 (8), 1569–1591.
- Liu, R.C., Liu, Y., Cai, Z.X., 2021. Influence of the growth gradient on surface wrinkling and pattern transition in growing tubular tissues. *Proc. R. Soc. Lond. Ser. A Math. Phys. Eng. Sci.* 477, 20210441.
- Liu, Y., Zhang, Z., Devillanova, G., Cai, Z., 2020. Surface instabilities in graded tubular tissues induced by volumetric growth. *Int. J. Non-Linear Mech.* 127, 103612.
- Moulton, D.E., Goriely, A., 2011. Circumferential buckling instability of a growing cylindrical tube. *J. Mech. Phys. Solids* 59, 525–537.
- Nguyen, N., Nath, N., Deseri, L., Edith Tzeng, E., Velankar, S.S., Pocivavsek, L., 2020. Wrinkling instabilities for biologically relevant fiber-reinforced composite materials with a case study of Neo-Hookean/Ogden-Gasser-Holzapfel bilayer. *Biomech. Model. Mech.* 19, 2375–2395.
- Ogden, R.W., Sotiropoulos, D.A., 1996. The effect of pre-stress on guided ultrasonic waves between a surface layer and a half-space. *Ultrasonics* 34, 491–494.
- Qi, L., Ruck, C., Szychalski, G., King, B., Wu, B.X., Zhao, Y., 2018. Writing wrinkles on poly(dimethylsiloxane)(PDMS) by surface oxidation with a CO₂ laser engraver. *ACS Appl. Mater. Interfaces* 10, 4295–4304.
- Sabbah, A., Youssef, A., Damman, P., 2016. Superhydrophobic surfaces created by elastic instability of PDMS. *Appl. Sci.* 6 (5), 152.
- Sanjarani Pour, M., 2010. WKB analysis of the buckling of a neo-Hookean cylindrical shell of arbitrary thickness subject to an external pressure. *Int. J. Appl. Mech.* 2 (4), 857–870.
- Sanjarani Pour, M., Fu, Y.B., 2002. WKB method with repeated roots and its application to the buckling analysis of an everted cylindrical tube. *SIAM J. Appl. Math.* 62 (6), 1856–1871.
- Sanjarani Pour, M., Hatami, A., Abdolalian, N., 2013. Another approach of WKB method for the stability analysis of the bending of an elastic rubber block. *Int. J. Eng. Sci.* 62, 1–8.
- Shield, T.W., Kim, K.S., Shield, R.T., 1994. The buckling of an elastic layer bonded to an elastic substrate in plane strain. *J. Appl. Mech.* 61 (2), 231–235.
- Shuvalov, A.L., 2003a. The Frobenius power series solution for cylindrically anisotropic radially inhomogeneous elastic materials. *Q. J. Mech. Appl. Math.* 56 (3), 327–345.
- Shuvalov, A.L., 2003b. A sextic formalism for three-dimensional elastodynamics of cylindrically anisotropic radially inhomogeneous materials. *Proc. R. Soc. Lond. Ser. A Math. Phys. Eng. Sci.* 459, 1611–1639.
- Song, J.T., Jiang, H.Q., Liu, Z.J., Khang, D.Y., Huang, Y., Rogers, J.A., Lu, C., Koh, C.G., 2008. Buckling of a stiff thin film on a compliant substrate in large deformation. *Int. J. Solids Struct.* 45, 3107–3121.
- Stafford, C.M., Harrison, C., Beers, K.L., Karim, A., Amis, E.J., Vanlandingham, M.R., Kim, H., Volksen, W., Miller, R.D., Simonyi, E.E., 2004. A buckling-based metrology for measuring the elastic moduli of polymeric thin films. *Nat. Mater.* 3, 545–550.
- Steigmann, D.J., Ogden, R.W., 1997. Plane deformations of elastic solids with intrinsic boundary elasticity. *Proc. R. Soc. Lond. Ser. A Math. Phys. Eng. Sci.* 453, 853–877.
- Stewart, P.S., Waters, S.L., El Sayed, T., Vella, D., Goriely, A., 2016. Wrinkling, creasing, and folding in fiber-reinforced soft tissues. *Extreme Mech. Lett.* 8, 22–29.
- Stroh, A.N., 1962. Steady state problems in anisotropic elasticity. *J. Math. Phys.* 41, 77–103.
- Su, Y.P., 2020. Voltage-controlled instability transitions and competitions in a finitely deformed dielectric elastomer tube. *Int. J. Eng. Sci.* 157, 103380.
- Su, Y.P., Wu, B., Chen, W.Q., Destrade, M., 2019. Finite bending and pattern evolution of the associated instability for a dielectric elastomer slab. *Int. J. Solids Struct.* 158, 191–209.
- Su, Y., Zhou, W.J., Chen, W.Q., Lü, C.F., 2016. On buckling of a soft incompressible electroactive hollow cylinder. *Int. J. Solids Struct.* 97–98, 400–416.
- Wang, J.W., Li, B., Cao, Y.P., Feng, X.Q., Gao, H., 2016. Wrinkling micropatterns regulated by a hard skin layer with a periodic stiffness distribution on a soft material. *Appl. Phys. Lett.* 108, 021903.
- Wang, G., Liu, Y., Fu, Y.B., 2023. A refined model for the buckling of film/substrate bilayers. *Math. Mech. Solids* 28 (1), 313–330.
- Wang, M., Mu, L., Zhang, H., Ma, S., Liang, Y., Ren, L., 2021. Flexible strain sensor with ridge-like microstructures for wearable applications. *Polym. Adv. Technol.* 33, 96–103.
- Wang, C.J., Zhang, S., Nie, S., Su, Y.P., Chen, W.Q., Song, J.Z., 2020. Buckling of a stiff thin film on a bi-layer compliant substrate of finite thickness. *Int. J. Solids Struct.* 188–189, 133–140.
- Wilder, E.A., Guo, S., Lin-Gibson, S., Fasolka, M.J., Stafford, C.M., 2006. Measuring the modulus of soft polymer networks via a buckling-based metrology. *J. Am. Chem. Soc.* 128 (12), 4138–4143.
- Wu, Z.G., Bouklas, N., Huang, R., 2013. Swell-induced surface instability of hydrogel layers with material properties varying in thickness direction. *Int. J. Solids Struct.* 50, 578–587.

- Wu, Z.G., Meng, J.X., Liu, Y.H., Li, H., Huang, R., 2014. A state space method for surface instability of elastic layers with material properties varying in thickness direction. *J. Appl. Mech.* 81 (8), 081003.
- Yang, S.Y., Chen, Y.C., 2017. Wrinkle surface instability of an inhomogeneous elastic block with graded stiffness. *Proc. R. Soc. Lond. Ser. A Math. Phys. Eng. Sci.* 473, 20160882.
- Yang, S., Khare, K., Lin, P.C., 2010. Harnessing surface wrinkle patterns in soft matter. *Adv. Funct. Mater.* 20, 2550–2564.
- Yin, J., Gerling, G.J., Chen, X., 2010. Mechanical modeling of a wrinkled fingertip immersed in water. *Acta Biomater.* 6, 1487–1496.
- Zhang, Z., Zhang, T., Zhang, Y.W., Kim, K., Gao, H., 2012. Strain-controlled switching of hierarchically wrinkled surfaces between superhydrophobicity and superhydrophilicity. *J. Am. Chem. Soc.* 28 (5), 2753–2760.
- Zhao, X., Wang, J., Huang, J., Li, L., Liu, E., Zhao, J., Li, Q., Zhang, X., Lu, C., 2020. Path-guided hierarchical surface relief gratings on azo-films induced by polarized light illumination through surface-wrinkling phase mask. *Langmuir* 36, 2837–2846.
- Zhou, M.T., Cai, Z.X., Fu, Y.B., 2022. Post-buckling of an elastic half-space coated by double layers. *Math. Mech. Solids* 27 (2), 193–209.